This document is confidential and is proprietary to the American Chemical Society and its authors. Do not copy or disclose without written permission. If you have received this item in error, notify the sender and delete all copies.

### **Understanding Control of Speciation of Molybdenum Oxides in MFI Type Zeolites**

Pil Type Zeontes			
Chemistry of Materials			
cm-2023-015457.R3			
Article			
n/a			
Hiennadi, Emanuele; Virginia Tech, Department of Chemical Engineering Molajafari, Fateme; Texas Tech University, Chemical Engineering Rana, Rachita; University of California Davis, Chemical Engineering Hoffman, Adam; SLAC National Accelerator Laboratory, SSRL Bare, Simon; SLAC National Accelerator Laboratory, SSRL Howe, Joshua; Texas Tech University, Chemical Engineering J. Khatib, Sheima; Virginia Tech, Department of Chemical Engineering			

# SCHOLARONE™ Manuscripts

Page 1 of 41

2

**Understanding Control of Speciation of Molybdenum Oxides in MFI Type Zeolites** 1 3 4 5 2 7 3 Emanuele J. Hiennadi<sup>1†</sup>, Fateme Molajafari<sup>2†</sup>, Rachita Rana<sup>3</sup>, Adam S. Hoffman<sup>4</sup>, Simon R. Bare<sup>4</sup>, Joshua 8 <sup>2,\*</sup>,

Sheima J. Khatib<sup>1,\*</sup>

- 4 D. Howe
- 5 10

- <sup>1</sup>Department of Chemical Engineering, Virginia Tech, Blacksburg, VA, 24061 12
- <sup>2</sup>Department of Chemical Engineering, Texas Tech University, Lubbock, TX, 79409 13
- 14
- <sup>3</sup>Department of Chemical Engineering, University of California, Davis, Davis, CA, 95616 15

Chemistry of Materials
16 8
17 9 <sup>4</sup> Stanford Synchrotron Radiation Lightsource, SLAC National Accelerator Laboratory, Menlo Park, CA, 18
19 10 94025
†E.J.H. and F.M. contributed equally to this work.
*Correspondence: joshua.d.howe@ttu.edu (J.D.H.); sheimajk@vt.edu (S.J.K.) 23 24 13 25
26 14 Abstract 27
28 15 Metal oxide-impregnated zeolites are employed in a wide variety of catalytic reactions, including in
29 16 methane dehydroaromatization (MDA). The most studied catalysts for MDA are Mo carbides supported 30
on H-ZSM-5, formed through carburization of Mo-oxide loaded H-ZSM-5. Complete structural
33 18 understanding of these materials has not yet been achieved, limiting the potential for rational catalyst
34 19 design for improved performance. We hereby pursue experimental and theoretical investigations of these 35
catalyst precursors to uncover rational design principles. We employ temperature-programmed oxidation
and extended X-ray absorption fine structure experiments, density functional theory calculations, and
40 22 QuantEXAFS analysis to unveil Mo-oxide speciation in H-ZSM-5. We demonstrate that Mo-oxides exist
41 23 within these systems as a combination of various motifs and the relative abundance of these species is 42
controlled through tailored preparation methods. The synergies exploited in this work may be leveraged through tailored preparation methods.
in other related catalysts. The conclusions drawn are applicable to other relevant applications of zeolite-
46 47 26 supported metal oxides.
48 49
50 Page 2 of 41
51

1 2		
3	1	
4		
5 6	2	
7	3	
		1. Introduction
		Zeolites are crystalline (alumino-)silicate nanoporous materials with precise topologies and well-
9	4	defined pores. Each zeolite possesses a particular pore architecture with specific channel diameters, 8 dimensionalities (1-3D and combinations thereof), cages, and pockets. Substitution of Si sites in the zeolite
10 11	5	framework by trivalent elements such as Al leads to a negative charge that is compensated by
12 13	6	extraframework cations. During synthesis, common cations are H <sup>+</sup> , Na <sup>+</sup> , or Ca <sup>2+</sup> , but these cations may be
14 15	7	postsynthetically exchanged with other species, including transition metals such as Fe, Co, Ni, and Cu.
16	8	The specific interaction between the extraframework cation, or cationic metal complex, and the trivalent
17 18	9	framework atom, as well as the confinement acquired by the metal cation based on its location within the
19 í 20	LO	zeolite pore structure, endows these metal-zeolite composites with unique properties that make them
21	11	active, selective, and stable catalysts in a variety of industrially and environmentally relevant reactions.
22 24 2 25		These reactions have applications in and beyond oil $refining^{[1,2]}$ , biomass conversion <sup>[3,4]</sup> , gas 23 valorization <sup>[5-8]</sup> , methanol to hydrocarbon conversion <sup>[9-11]</sup> , and NO <sub>x</sub> selective reduction <sup>[12-16]</sup> .
26 í 27	L4	To establish rigorous structure-activity relations in metal-zeolite catalysts, it is of utmost importance
28 í 29	15	to be able to characterize the local structure of these dispersed metal cation complexes within zeolite
30 í	L6	channels. This task has proven to be complicated given both the dispersion of the metal sites and the added
32	17	complexity derived from the zeolite structure and texture. As with most catalytic materials, the most
33	18	promising route to obtain rigorous structural characterization of metal-zeolite catalysts is by applying
51 52 53 54 55 56 57 58		
EΩ		2

34		
35 1 36	.9	various relevant characterization techniques in concert with computational calculations. This integrated
37	20	approach is especially valuable given that the synthesis techniques employed in preparation of metal-
38 39	21	zeolite catalysts (by incipient wetness impregnation, ion exchange, or solid-state ion exchange) do not
40 2 41	22	usually allow for strict control of the metal speciation, leading to coexistence of multiple species within
42 2 43	23	the zeolite pores. In this work we demonstrate a strategy to study such systems through combined
	24	experimental and computational efforts with focus on the specific example of the Mo/H-ZSM-5
45 47 2 48		(framework type MFI) catalysts employed in methane dehydroaromatization (MDA). MDA is a single46 step, non-oxidative reaction that directly converts methane into liquid aromatics, light hydrocarbons, and
49		27 hydrogen as a co-product. MDA has drawn interest for its potential as a technology capable of converting
50	28	methane into transportable liquid products to reduce flaring of natural gas <sup>[5, 6, 17-20]</sup> .
	29 N	Molybdenum oxides dispersed within H-ZSM-5 channels are the most effective catalysts known to30 date for
	MD	OA. Under the relevant conditions, the starting Mo-oxide species migrate into the zeolite 31 channels and
		hor at Brønsted acidic sites (BAS) to form local anchored Mo-oxides. Upon exposure to
Page	e 3 o	f 41
1 2		
3 4	1	methane under reaction conditions, the anchored Mo-oxides reduce and carburize to form Mo carbides
5 6	2	and oxycarbides, which are generally accepted to be the active centers for MDA, although the details of
7		3 the reaction mechanism are yet unclear. Presently, there is debate on whether the MDA reaction proceeds
8 9		<ul> <li>[6], where the carbidic Mo centers activate methane to produce C<sub>2</sub>H<sub>x</sub></li> <li>4 via a bifunctional mechanism</li> </ul>
51 52 53		
54 55		
56		
57 58		
59		3

2		
3	1	
4		
5	2	
6	2	
7 10	3	5 intermediates that subsequently undergo aromatization to benzene on
		the BAS of the zeolite, or a
11 12	6	monofunctional mechanism <sup>[6, 21]</sup> , where the carbidic Mo is responsible for both the methane activation
13	Ū	, where the curvate in responding to the inclination and water
14 15	7	and also CH <sub>x</sub> species aromatization to benzene. The exact Mo speciation at different stages of MDA also
16	8	remains a point of debate in literature. Understanding the true nature of the Mo species throughout the
17 18	9	entire catalyst life cycle will help elucidate the reaction mechanism for MDA and in turn facilitate rational
19		design of more stable, commercially viable catalysts. Starting supported Mo-oxides have been reported to
20		+ monomers[5, 18, 22-27], MoO22+ monomers[5, 18, 22, 23, 26-32], or Mo2O52+ dimers[5, 17, 22, 24, 25, 27, 29,
21		11 be MoO <sub>2</sub> OH
22		12 31-37]. Gao et al. <sup>[18, 26]</sup> studied the identity and anchoring site of the initial Mo-oxide monomer structures
23		
24 2	L3	by combining density functional theory (DFT) with multiple spectroscopic techniques such as in situ
25 26 2	1 /1	Raman spectroscopy and in situ UV-vis to report the MoO <sub>2</sub> OH <sup>+</sup> and MoO <sub>2</sub> <sup>2+</sup> structures. On the other
20 . 27	L4	Raman spectroscopy and in situ 0 v vis to report the MoO <sub>2</sub> O11 and MoO <sub>2</sub> structures. On the other
	15	hand, using Raman and X-ray absorption spectroscopy (XAS), together with quantification of water
29 30	16	formed during a temperature-programmed oxidation of the catalyst precursors, existence of $Mo_2O_5{}^{2+}$
31 í 32	L7	dimeric species formed from condensation of two anchored MoO <sub>2</sub> OH <sup>+</sup> monomers was suggested <sup>[22, 25]</sup> .
	18	Herein we analyze closely the speciation of the anchored Mo-oxides in the starting Mo/H-ZSM-5 MDA
34	19	catalysts to clarify the differences observed in the literature regarding these structures.
51		
52		
53		
54 55		
56		
57		
58		
59		4
60		ACS Paragon Plus Environment

One important factor that could explain discrepancies in proposed Mo-oxide structures is the synthesis

technique employed in the preparation of the Mo/H-ZSM-5 catalysts. Groups reporting the presence of a

Mo<sub>2</sub>O<sub>5</sub><sup>2+</sup> dimer generally prepare the catalysts by "physical mixing" where MoO<sub>3</sub> powder and H-ZSM-5

are first mixed and ground, and then calcined [22]. The calcination step is crucial to enable the MoO<sub>3</sub> phase

to first spread over the external zeolite surface forming MoO<sub>x</sub> moieties that upon further heating above

the sublimation point migrate into the zeolite channels where they anchor at the BAS. Alternatively,

research groups reporting presence of anchored MoO<sub>2</sub><sup>2+</sup> monomers often employ incipient wetness impregnation to incorporate Mo onto the zeolite. This is done by adding a precisely measured volume of

an aqueous solution of the Mo-oxide precursor (usually ammonium heptamolybdate tetrahydrate (AHM)) 28
29 to the H-ZSM-5 support. The solution is added dropwise until reaching the incipient wetness point. The 30
fact that groups preparing catalysts by these different synthesis techniques have generally presented 31 evidence
for different Mo-oxide speciation inevitably leads to questions of whether differences in the

Page 4 of 41

chemistry involved in the synthesis procedures subsequently affect the metal oxide speciation. We have not been able to identify in the published MDA literature any work that has contrasted catalyst structures employing the different synthesis techniques.

- 9 4 To deconvolute the discrepancy between conflicting reports of Mo-oxide structure on Mo/H-ZSM-5,
  - in this work we investigate the  $MoO_x$  speciation as a function of the synthesis technique by exploring
  - 6 catalysts synthesized by the two most employed methods in the literature, physical mixing of MoO<sub>3</sub> with
  - 7 H-ZSM-5 and incipient wetness impregnation of Mo-oxide precursors on H-ZSM-5. We employ a

1 2			
3	1		
4	1		
5	2		
6	2		
7 16	3 8	combination of experimental and computational techniques to evaluate the speciation of MoO <sub>x</sub> on H-	
17 18	9	ZSM-5. We have characterized the stoichiometry of the anchored Mo-oxides in the catalysts prepared by	
19 : 20	10	both techniques indirectly via temperature-programmed calcination of Mo/H-ZSM-5 precursors under	
21	11	oxidative conditions while quantifying the water evolution resulting from the reaction of the molybdenum	1
22 24 : 26 : 27		oxide precursors (we will refer to these as temperature-programmed oxidation, TPO, experiments). The 23 quantity of water produced in the process can aid in determining the stoichiometry of the anchored Mo25 oxides. We also report direct measurements of the structure of the molybdenum species using operandom oxides.	
28	15	XAS. We have monitored the average local electronic structure, X-ray absorption near-edge structure	
29 30	16	(XANES), of the Mo species as they evolve from the precursors to the anchored species during the	
31		tempera ure- programm ed oxidation while monitorin the samp temperatu e and wate produced during [38, 39], and	n le ir er
33		18	
51 52 53 54 55 56 57		the TPC	).
58			6
59			0

		spectral deconvolut ion methods, principal component analysis (PCA)
34		multivari ate curve resolutionalternating least squares (MCR-ALS) <sup>[38, 39]</sup> , were used to identify the
35 36 20 37	evolution of species during the TPO. Local atomic structure, extended X-ray absorption	on fine structure
38		(EXAFS), was recorded after the TPO for analysis described below. In parallel, we have performed DFT
39 40		+ and MoO <sub>2</sub> <sup>2+</sup> 22 calculatio ns focused on the electronic
51 52 53 54 55 56 57		
58 59 60	ACS Paragon Plus Environment	7
	Aco i diagoni i las Environniche	

priori

A

1			
2			
3	1		
4			
5	2		
6 7	3		
•	J		structure,
			location, and
			stability of the
			$MoO_2OH$
41			23
			monomer
			s and $Mo_2O_5^{2+}$
			dimers
			anchored on
			single and double Al-
			atom
			framework
			sites inside H-
			ZSM42
43 44	24	5 to assess the viability of specific structures. These calculations provide atomistic charac	terization of the
45 46	25	nature and location of these motifs and enable comment on their thermodynamic viabilities	es. We include
47	26	in this set of calculations evaluation of anchoring possibility of Mo-oxides in proximity of H	3AS without
48 49	27	direct coordination, identifying viable motifs not previously considered in the literature. We	combine our
50	28	DFT-based structure models with our XAS-measured spectra through QuantEXAFS analy	sis <sup>[40]</sup> to identify
	29	which specific structures among those we have computed best agree with our measured spec	etra and how 30
	the	e structures that best agree vary in motif as a function of metal loading and catalyst prepara	tion method. 31
	Th	arough this combined theoretical and experimental investigation, we conclude that specific me	otifs of
Pag	ge 5 d	of 41	
51			
52			
53			
54			
55 56			
57			
58			
E0			Q

1 2			
3	1	Mo-oxide catalyst precursors may be promoted or inhibited through system choice and preparati	ion.
-	Fur 3	thermore, the strategy we develop here may be extended to other transition metal-zeolite systems 6 involving presence of dispersed metal-oxides within zeolite channels.	
10	4	2. Methods	
11 12 13	5	2. 1. Experimental Methods	
14 15	6	2.1.1. Catalyst preparation – Physical Mixing & Incipient Wetness Impregnation	
16 17	7	The H-ZSM-5 support was prepared by calcining NH <sub>4</sub> -ZSM-5 (Si/Al = 15 and 40, Zeolys	t
18	8	International) at 500 °C for 6 h. Each of two methods, physical mixing (PM) and incipient wetness	
19 20	9	impregnation (IWI), were used to prepare two sets of Mo/H-ZSM-5 catalysts. For PM catalysts, mixt	ures
21 1 22	.0	of MoO <sub>3</sub> (Sigma Aldrich, 99.9%) and H-ZSM-5 were ground by hand in an agate mortar and pest	le for
23 1 24	.1	approximately 0.5 h, reducing the mixture to a powder to ensure maximum contact between the Mo	o-oxide
25	12	and the H-ZSM-5 support. For IWI catalysts, first the incipient wetness point for a certain mass of H-	-
26 27	13	ZSM-5 was first determined with water. For this, water was added drop by drop to the H-ZSM-5 until	1
28 1 29	.4	reaching the incipient point whereby the zeolite was wet but did not possess any supernatant water	r. The
30	15	incipient point volume was then used to calculate the volume of aqueous solution of ammonium	
31 32	16	heptamolybdate tetrahydrate ((NH <sub>4</sub> ) <sub>6</sub> Mo <sub>7</sub> O <sub>24</sub> ,4H <sub>2</sub> O, Sigma Aldrich) to be added to the H-ZSM-5 sup	port
33 1 34	.7	for the different catalyst samples. After impregnation, the samples were dried overnight at ambi	ent
35			18 c
			ondit ions.
51			
52 53			
54			
55 56			
57			
58			

51 52 53

54 55

56 57 58

59

60 AG

meth ane arom atiza tion react ions, the two sets of catal ysts were calci ned unde r two [18, 22, 19 di ffere nt temp eratu re ramp profi les follo wing the

For

edur es empl oyed previ ousl y in the litera ture 20 38 41] . For PM catal ysts, the asprep ared catal ysts were calci ned to 350 °C, held for 2 h, and ramp ed to 700 39 °C all at 10 °C min<sup>-1</sup>. For IWI catalysts, the as-prepared catalysts were calcined to 200 °C, held for 3 h, 40 21 41 ramped to 500 °C, held for 2 h, all at 10 °C min<sup>-1</sup>. **Table 1** details the established nomenclature for the 42 22 43 51 52 53 54 55 56 57 58 11 59

proc

44 23 Mo/H-ZSM-5 samples used in this study. The nomenclature uses the following format: A-Mo/Z-B (C), 45 24 where A denotes the nominal Mo/Al ratio in the catalyst tenfold, B denotes the synthesis technique (PM 46 vs. IWI), and (C) denotes the Si/Al ratio of the support. 47 25 49 26 50 27 

Table 1. Nomenclature of prepared Mo/H-ZSM-5 samples reflecting metal loading, synthesis method.

			Nominal Mo	o/Al
8	Nomenclature	Mo wt.%	Ratio	Mo Precursor
9	1-Mo/Z-PM (15)	1	0.11	MoO <sub>3</sub>
10	1 1110/2 1111 (10)	•	0.11	111003
11	3-Mo/Z-PM (15)	3	0.34	MoO <sub>3</sub>
12	, ,			
13	4-Mo/Z-PM (15)	4	0.45	$MoO_3$
14	1-Mo/Z-PM (40)	0.4	0.11	MoO <sub>3</sub>
15	1-1/10/2-1 WI (40)	0.4	0.11	10003
16	3-Mo/Z-PM (40)	1.2	0.34	$MoO_3$
17				
18	4-Mo/Z-PM (40)	1.6	0.45	$MoO_3$
19 20	1-Mo/Z-IWI (15)	1	0.11	$AHM^*$
21				
22	2-Mo/Z-IWI (15)	2	0.22	AHM
23 24	3-Mo/Z-IWI (15)	3	0.34	AHM
25				
26	4-Mo/Z-IWI (15)	4	0.45	AHM
1 * 4HM - 4mmonium				

7 1 \* AHM = Ammonium

-Heptamolybdate

**Tetrahydrate** 

# 2 2.1.2. Quantitative Temperature-Programmed Oxidation (TPO)

Temperature-programmed oxidation of the Mo/H-ZSM-5 precursors (H-ZSM-5 with MoO<sub>3</sub> for PM

1
2
3
4
5
6
7
33

43 10 

- 4 samples, and H-ZSM-5 with ammonium heptamolybdate tetrahydrate for IWI samples) was performed in
- 5 a fixed-bed quartz reactor (8 mm i.d.) at atmospheric pressure and varying temperature programs for the
  - 6 different catalyst types as described in **Table 2**. The reactor was charged with 0.3 g of catalyst powder
    - 7 held in place by quartz wool. The catalyst precursors were heated to reaction temperature at a rate of 10
    - <sup>-1</sup> under a flow of 20% O<sub>2</sub> in Ar at a flow of 50.0 ml min<sup>-1</sup> and at different temperature profiles for
    - 8 °C min
    - 9 catalysts prepared via different synthesis methods. Evolution of  $H_2O$  signals (m/z = 18) during the TPO 42
    - experiment was monitored with a MKS Cirrus 3 atmospheric gas analyzer.

Table 2. Temperature profiles employed in TPO of Mo/H-ZSM-5 prepared with different synthesis methods.

Temperature Profile Segment	Physical Mixing (PM)	Incipient Wetness Impregnation (IWI)
1.	25 to 350 °C (10 °C min <sup>-1</sup> )	25 to 200 °C (10 °C min <sup>-1</sup> )
2.	hold 2 h	hold 2 h
3.	350 to 700 °C (10 °C min <sup>-1</sup> )	200 to 500 °C (10 °C min <sup>-1</sup> )
4.	<del>-</del>	hold 2 h
5.	-	500 to 700 °C (10 °C min <sup>-1</sup> )

Page 7 of 41

1 2.1.3. X-Ray Diffraction (XRD)

1		
2		
3	1	
4		
5		
6		
7		
34		
35	18	For IWI catalysts, the as-prepared catalysts were heated to 200 °C, isothermally held until no further
36	19	spectral changes were observed, ramped to 400 °C, held until no further spectral changes were observed,
37		
38	20	then ramped to 700 °C all at 10 °C min <sup>-1</sup> in a flow of 10 sccm of 20% O <sub>2</sub> /He. The composition of the
39		

- 40 21 effluent gas from the experimental cell was monitored using a Hiden QGA mass spectrometer.
- 41 22 2.1.5. XAS Analysis

- Transient XAS data and XANES spectra were processed (energy calibrated, normalized, interpolated to a
- 45 24 common energy grid) and correlated to the mass spectrometer data using CatXAS<sup>[43]</sup>. The normalized 46 <sup>[38, 39]</sup>. The data
- 47 25 XANES spectra were analyzed using PCA and MCR-ALS spectral deconvolution codes
- 48 26 range used during the PCA and MCR-ALS analysis was 19,925-20,250 eV with non-negative spectra and 49 non-negative concentration constraints applied during the MCR-ALS analysis.
  - 28 Steady-state EXAFS data were processed using Athena and QuantEXAFS<sup>[44, 40]</sup>. Athena was used for 29 energy calibration, normalization, merging of spectra to improve signal-to-noise, and EXAFS extraction.

Page 8 of 41

### 2.2. Computational Methods

#### 2 2.2.1. Calculations Details

8	3	Fully periodic DFT calculations were performed with a planewave basis set within the Vienna ab initio
9	[45	<sup>1</sup> (VASP) to study the speciation of Mo-oxide structures within H-ZSM-5. All spin10 4 simulation package
11 12		polarized DFT calculations used projector augmented wave pseudopotentials <sup>[46]</sup> and the generalized 5
13 14		6 gradient approximation of Perdew, Burke, and Ernzerhof (PBE) <sup>[47]</sup> . The planewave basis set cutoff energy
15	7	was 700 eV, and the reciprocal-space integration of the Brillouin zone was sampled at $\Gamma$ (1 × 1 × 1
16 17	8	Monkhorst-Pack grid). The atomic positions were optimized until interionic forces were less than 0.03
18 19 20	9	eV/Å in all Mo-oxide/H-ZSM-5 structures.
21 1 22	0	2.2.2. Models of Mo-oxides/H-ZSM-5 (Model details)
23 1 24	1	To generate models of $MoO_x$ species supported by H-ZSM-5, we began by optimizing the ZSM-5 unit
25	12	cell geometry using DFT, starting from a structure obtained from the International Zeolite Association
26 27	13	(IZA) database <sup>[48]</sup> . The ZSM-5 unit cell contains 288 atoms: 96 Si atoms and 192 O atoms. In ZSM-5,
28 1 29	4	each Si <sup>4+</sup> ion is charge-balanced by two O <sup>2-</sup> ions, and each Si <sup>4+</sup> ion is coordinated tetrahedrally by four
30		15 O <sup>2-</sup> . Isostructural substitution of one Si <sup>4+</sup> ion by an Al <sup>3+</sup> ion creates a local charge of -1, which is balanced
31		<sup>+</sup> ion) bound to an oxygen ion coordinated
32		16 by introducing a charge- compensating Brønsted acidic proton (H
33		17 to the Al <sup>3+</sup> species to generate H-ZSM-5. The ZSM-5 unit cell contains 12 chemically/coordinatively
34	0	
35 1 36	8	distinct tetrahedral sites (T-sites). H-ZSM-5 can be synthesized in various Si/Al ratios wherein a fraction
51 52 53 54 55 56 57		
56 59		17

2	
3 1	
4	
5 6	
7	
37 19	of the Si is substituted with Al and a charge-compensating proton <sup>[49-51]</sup> . Models of MoOx/H-ZSM-5 38
[18, 22, 2	within the DFT-optimized unit cell
39 20	structures were constructed with a variety of proposed motifs
	of H-ZSM-5. To select motifs for Mo-oxide speciation at the initial stages of methane 41 dehydroaromatization, the three most frequently spectroscopically evidenced proposed motifs of Mo-
	, MoO2OH+[18, 26], MoO22+[18, 29], and Mo2O52+[22, 29], were considered. In general, 44 23 oxides in the erature
45 <b>24</b> 46	we categorize $MoO_x$ species into two main categories: "Mo monomer" and "Mo dimer" species. $MoO_x$
47 25 48	species are proposed to anchor in the vicinity of Al-atom framework sites, with isolated Al sites allowing
49	formation only of MoO <sub>2</sub> OH <sup>+</sup> Mo monomer species and two A sites near one another additionally
50	<sup>2+</sup> Mo monomer species and Mo <sub>2</sub> O <sub>5</sub> <sup>2+</sup> Mo dimer species.
27	facilitating existence of both MoO <sub>2</sub>
28	The electronic structure and stability of the MoO <sub>2</sub> OH <sup>+</sup> monomer motif anchored on each of the 10
29	isolated symmetrically unique Al-substituted T-sites around a single 10-member ring in the straight
30	channel of H-ZSM-5 were explored, with the previously published DFT-calculated geometry of
F.1	
51 52	
53	

2

7

51 52 53

59 60

MoO <sub>2</sub> OH <sup>+</sup> used to	initialize calculations <sup>[1]</sup> . To date, studie	s of Mo-oxides anch	ored in zeolites have
focused on anchoring	g at expected strongly binding acidic si	tes <sup>[18, 22, 26, 28, 52]</sup> . We	have considered these

ca ses of  $MoO_2O$  $H^+$ anchored at (bidentat ely atop the T-site at which the Al cation is sited) or  $near\, Al^{3+}$ <sup>3+</sup> site) as 4 si tes (sharing least at one of two bidentate bonds with an oxygen directly

> coordinat ed to the

Al

2	
3	1
4	
5	2
6 7	3
10	5
	well as the potential for these oxides to anchor elsewher e in the zeolite to investiga te the viability of such
11	
12 13	anchoring motifs. Because structures with greater separations between the Mo and Al <sup>3+</sup> are not expected
14	7 to be thermodynamically favored, we have limited this study to two complementary investigations: either
15	<sup>3+</sup> at T-site 8 with the other varying between all unique T-sites within the 10168 the Mo-oxide or the Al
17 18	9 member ring. The various structural arrangements of siting both the MoO <sub>2</sub> OH <sup>+</sup> and the Al <sup>3+</sup> within the
19	10 zeolite in this work are illustrated in <b>Figure 1</b> . The energetics of these structures represented as a matrix
20 21	<sup>+</sup> species anchored atop the Al-substituted Si sites as the diagonal 11 are provided in <b>Figure 9</b> with MoO <sub>2</sub> OH
22	12 elements of this matrix. The elements not along the diagonal of this matrix represent the possibility of
23 24 1	anchoring of the Mo monomer atop Si sites near to or distant from the Al atom inside the zeolite's
51 52 53 54 55 56 57 58	
59	20

31 17

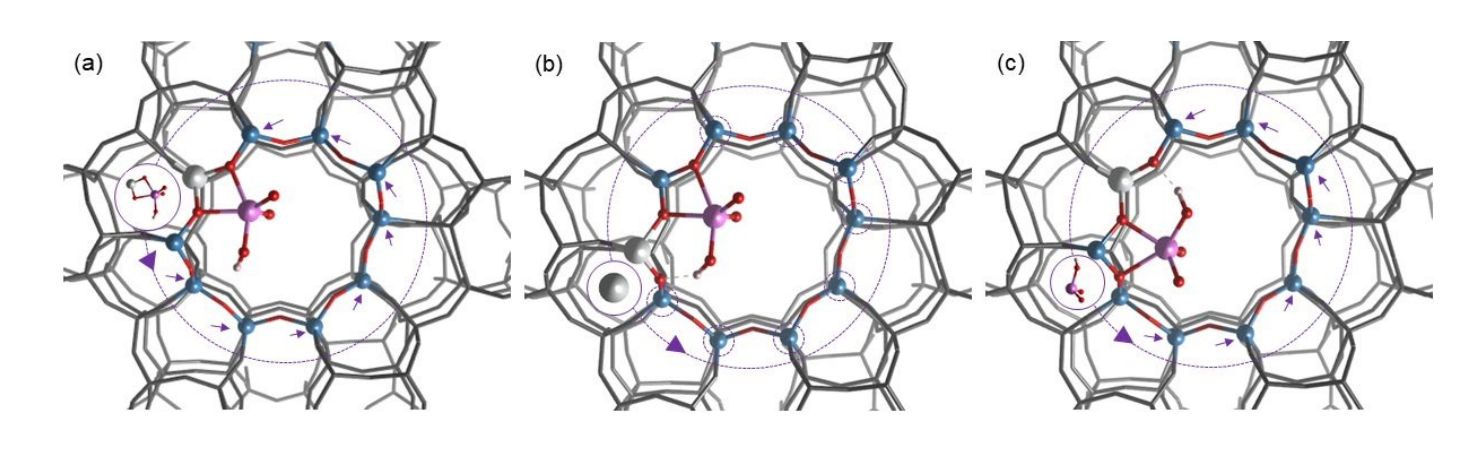
14 channels, with distance from the diagonal representing a greater coordinative distance between Al site and

<sup>+</sup> anchoring site around the 10-member straight channel ring of H-ZSM-5. Inclusion of these 15 MoO<sub>2</sub>OH

16 motifs in our structure database allows for assessment of whether these species may be likely contributors

to observed EXAFS spectra. 32

We have also studied the other Mo-oxide motifs to exist within H-ZSM-5, noting that these motifs,



48 Figure 1. Schematic of: (a) MoO<sub>2</sub>OH<sup>+</sup> monomer anchored atop the Al atom-substituted T-site demonstrating 49 potential T-sites for "atop" anchoring. (b) MoO<sub>2</sub>OH<sup>+</sup> monomer anchored at T-site 8, demonstrating potential other 50 T-sites for Al substitution. (c) MoO<sub>2</sub>OH<sup>+</sup> monomer anchored adjacent to the Al-substituted T-site demonstrating potential for anchoring both near to and distant from the Al-substituted T-site. Color scheme: silicon (blue), oxygen (red), aluminum (silver), molybdenum (magenta), hydrogen (white), non-specific framework (grey).

19 MoO<sub>2</sub><sup>2+</sup> and Mo<sub>2</sub>O<sub>5</sub><sup>2+</sup>, each require two Al<sup>3+</sup> sites and two acidic protons to exist in proximity to one 20 another within the H-ZSM-5 pore to anchor to the H-ZSM-5 framework. Consistent with previous studies

Page 10 of 41

2		
3	1	
4		
5	2	
6	2	
7	of these motifs, the possible double Al-atom framework sites in H-ZSM-5 were considered as Al-O	-Si-
$\Omega$	Al (Next-Nearest-Neighbor, NNN), and Al-O-(Si-O) <sub>2</sub> -Al (Next-Next-Nearest-Neighbor, NNNN) <sup>[14, 16, 19]</sup> ,	
		anu
	choring of this second type of Mo monomer $(MoO_2^{2+})$ as well as the Mo dimer $(Mo_2O_5^{2+})$ on 8	
9	4 candidate double Al sites inside the straight and sinusoidal channels of H-ZSM-5 were investigated.	
10 11	5 Because the addition of siting of one more Al <sup>3+</sup> provides an additional combinatoric (although proximal	ly
12		6
		c
		on str
		ai
		ne
		d) de
		gr
		ee
		of fre
		ed
		o
		m,
		we si
		m
		pli
		fy th
		e
		se
		ar ch
51		CII
52		
53 54		
54 55		
56		
57		

in g sp ac e by co nsi de rin g on ly a li mi te d su bs et of [29] 7 p os sib le str uc tur es.  $\mathbf{W}$ e m ak e ou r ch oi ce

13

14

57 58

59

> uc tur es to stu dy fol lo wi ng th e W or k of Zh

of  $\mathbf{W}$ hi ch str

[18]

ou et al.

W e co nsi de

51

15

58

59 60

r a set of ei gh t M o  $O_2$ sp eci es an ch or ed at va rio us Al Al pa irs (8, 11 8, 12 16 8 a nd Ga o et

9 6,9; 6,6; 3,12; 3,3; 1,10; 1,1, where these pairs of numbers denote the T-sites at which the  $Al^{3+}$  cations are

51 52 53

17 18

> 54 55 56

> 57 58

59

60 ACS Paragon Plus Environment

al.

1 2		
3	4	
4	1	
5	2	
6	•	
7 19	3	10 sited, following nomenclature in <b>Figure 8 (a)</b> ) inside the straight and sinusoidal channels of H-ZSM-5. It
20		<sup>2+</sup> species, the anchoring site of the Mo atom is not fully
21		species, the distribution is not fairly should be noted that for some of the $MoO_2$
22		12 specified by knowing at which T-sites Al atoms are substituted, necessitating the nomenclature described
<ul><li>23</li><li>24 1</li><li>25</li></ul>	.3	subsequently for uniquely identifying these structures. For Mo <sub>2</sub> O <sub>5</sub> <sup>2+</sup> dimers, we have additionally
26 1	.4	considered the possibility that the larger structure may be anchored at double Al sites (3,7; 3,8; 2,8; and
27	15	2.7) with greater accordinative congretion (next next next news) neighbor NNININI or "fourth negrees"
28	15	2,7) with greater coordinative separation (next-next-nearest-neighbor, NNNNN, or "fourth nearest-
29 30	16	neighbor", for instance). In total, 42 models of $MoO_2OH^+$ , 8 models of $MoO_2^{2+}$ , and 12 models of $Mo_2O_5^{2+}$
31		17 were considered in this work, with differences between models of like stoichiometry being the T-sites at
32		<sup>3+</sup> is substituted within the framework. To
33		18 which they are anchored as well as the T-sites at which Al
34		19 uniquely identify each of the 62 structures, we introduce the following nomenclature system:
35		For MaQ-QU+ managers, we use MaQ-QU+ 4. At P, where 4 denotes the anchoring site of Ma, avide
36 2 37	20	For MoO <sub>2</sub> OH <sup>+</sup> monomers, we use MoO <sub>2</sub> OH <sup>+</sup> -A, Al B, where A denotes the anchoring site of Mo-oxide
38		and <i>B</i> denotes the Al-substituted T-site.
51 52 53 54 55		
56 57		
58		
59		26

39 40		monomers, we use $MoO_2^{2^+}$ - $A$ - $B$ (Al $C$ , $D$ ), where $A$ and $B$ denote the sites between which For $MoO_2$
41 42		the Mo atom is anchored and C and D denote the Al-substituted T-sites.
42 43 2 44	24	For $Mo_2O_5^{2+}$ dimers, we use $Mo_2O_5^{2+}$ - $A$ , $B$ (Al $C$ , $D$ ), where $A$ and $B$ denote the sites atop which the
45 2 46	25	Mo is bidentately anchored and $C$ and $D$ denote the Al-substituted T-sites.
47 2	26	Adsorption Energetics of Mo-oxide in H-ZSM-5 48
49 2 50	27	Binding energies of MoO <sub>x</sub> species in H-ZSM-5 were calculated to investigate their thermodynamic
	28	viabilities; the same theory level as for geometry optimization has been applied in these calculations. We 29
	hav	we investigated the binding energies of Mo-oxide species referenced to MoO <sub>3</sub> in the gas phase. While
Pag	30 e 11	$\mbox{MoO}_3$ in the gas phase is expected to be thermodynamically unfavored and therefore lead to highly of 41
1		
3 4	1	exothermic values for anchoring of MoO <sub>x</sub> species within H-ZSM-5, we focus our discussion on the relative
5 6	2	energetics between these species such that this reference choice has no bearing on the conclusions drawn.
7 8	3	To calculate the reference energy of MoO <sub>3</sub> and H <sub>2</sub> O, an isolated MoO <sub>3</sub> or H <sub>2</sub> O unit was simulated in a 20
9	4	$\times$ 20 $\times$ 13.5 Å box such that interaction between periodic images of the molecules does not contribute
10 12 13	5 6	significantly to energetics. For the reference energy of the H <sub>2</sub> O molecule, corrections to the potential to 11 account for the permanent electrostatic dipole of H <sub>2</sub> O were included.
14 15	7	The adsorption energy of the Mo monomer anchored at a single Al-atom framework site was
16	8	calculated using:
17 18	9	$\Delta EE = EE_{HH-ZZZZZZ-5+ZZMMOO_2OOHH^+} - EE_{HH-ZZZZZZ-5} - EE_{ZZMMOO_3} $ (1)
51 52 53 54 55 56 57 58		

```
1
2
3
     1
     2
5
        where {}^{EE}_{HH-ZZZZZZ-5+ZZMM00_200HH+}, EE_{HH-ZZZZZZZ-5}, and EE_{ZZMM00_3} denote the energies of H-ZSM-5-plus-
MoO_2OH^+
20
21 11 complex, bare H-ZSM-5, and MoO<sub>3</sub>, respectively. A negative \Delta EE in this convention corresponds to an 22
          exothermic adsorption.
23 12
24
25 13 In a similar calculation, the adsorption energetics of the Mo monomer anchored at double Al site was
    14 calculated as follows:
27
28 15 \Delta EE = EE_{HH-ZZZZZZ-5+ZZMM002} <sup>2+</sup> + EE_{HH200} - EE_{HH-ZZZZZZ-5} - EE_{ZZMM003}
                                                                                                   (2)
30 16 where EE_{HH-ZZZZZZ-5+ZZMM002} 2+, EE_{HH-ZZZZZZ-5}, and EE_{HH200} denote the energies of H-ZSM-5-plus-MoO2<sup>2+</sup>
complex,
31
           bare H-ZSM-5 containing two Al atoms, and water, respectively.
32 17
33
34 18 Finally, to study the stability of the Mo dimer, equation (3) was employed.
35 19 \Delta EE = EE_{HH-ZZZZZZ-5+ZZMM_2OO_5}^{2+} + EE_{HH_2OO} - EE_{HH-ZZZZZZ-5}^{2-} - 2 \times EE_{ZZMMOO_3}^{2-}
                                                                                                                   (3)
36
37 20 where ^{EE}_{HH-ZZZZZZ-5+ZZMM_2OO_5} 2+ aaaaaa EE_{HH-ZZZZZZ-5} denote the energies of H-ZSM-5-plus-Mo<sub>2</sub>O<sub>5</sub><sup>2+</sup> complex
and
38
        bare H-ZSM-5 containing two Al atoms, respectively. 40
39 21
               In all cases above, we have referenced energies against one particular H-ZSM-5 structure. In reality,
41 22
42
             for a given Al siting arrangement with N Al sited according to Lowenstein's rule, there are 4<sup>N</sup> unique
43 23
44
51
52
53
54
55
56
57
58
59
```

- Chemistry of Materials 24 sitings of acidic protons, some of which are more favorable than others. We have investigated the 25 magnitude of the effect of proton siting and found it to be small relative to an aribtrary H-ZSM-5 model. 47 26 We computed the energy of the H-ZSM-5 48 structures with the charge-compensating proton bound to each <sup>3+</sup> cation, which we used to calculate the Boltzmann 49 27 of the four unique oxygen atoms coordinated to 50 the Al average energy (for this we have used the reaction operating temperature of T = 973.15 K) using equation 28
  - 29 (4). The H-ZSM-5 structure energies were predicted to range from 6.6 kJ mol<sup>-1</sup> less stable to 2.5 kJ mol<sup>-1</sup>
  - 30 more stable than the Boltzmann average for a single Al-substituted T-site. To study effects of Boltzmann

Page 12 of 41

averaging on H-ZSM-5 with two Al atoms, we consider H-ZSM-5 with Al substituted at T-sites 3 and 12, a NNN (Al-O-Si-O-Al) arrangement which we expect to be the upper bound of deviation from the single-Al case due to proximity of the Al<sup>3+</sup> cations. We considered the 16 chemically unique arrangements for

<sup>-1</sup> less stable to 7.7 kJ mol<sup>-1</sup> more stable 8

proton siting and calculated

energies ranging from 55.7 kJ mol

5 than the Boltzmann average. We note that the system predicted to be ~56 kJ mol<sup>-1</sup> less stable for siting of

acidic protons is not representative of the typical systems and features acidic protons sited in proximity to 6 12

one another with NNN Al siting and would not be expected to contribute with a high probability to

observed states. 8 16

10

11

13

14 15

60

1		
2		
3	1	
4 5	2	
6		
7 19	3	
20		
21 1	LO	where $EE_{ii}$ and $\Delta EE_{ii}$ denote the energies of H-ZSM-5 configuration $i$ , and the relative energy of
22 1 23	l1	configuration $i$ to the ground-state configuration, respectively.
24 12 25	2	2.2.3. DFT-based EXAFS analysis (QuantEXAFS)
26 13 27	3	The EXAFS data were analyzed with the QuantEXAFS <sup>[40]</sup> workflow that uses the X-ray Larch package <sup>[53]</sup> .
28 1	L4	QuantEXAFS is an automated workflow for EXAFS analysis that uses a library of DFT-optimized
29 1 30	L5	structures to generate feff.inp files and model the EXAFS data. The code uses Seaborn and Matplotlib for
31 16 32	ô	plotting the fitting results. Assuming the database of DFT-optimized structures was exhaustive, the
33		17 coordination numbers were 'fixed' in EXAFS analysis and were not included as a fit parameter unlike the
34 35		conventional method. Additionally, all the scattering paths generated using FEFF were categorized based 18
36		19 on distance-dependent variables ( $\sigma_i^2$ and $\alpha_i$ ) and used in the fit. Unique values of D-W factors ( $\sigma_i^2$ ) and $\alpha_i$
37 38 20	)	(fixed error correction allowed in DFT-generated bond distances) were generated for each category of
39 40 21	l	paths and used in the model.
41 42		
43 22	2	3. Results
44		
51		
52		
53 54		
55		
56 57		
58		
59		30

### 45 23 3.1. Quantitative Temperature-Programmed Oxidation

46 24 We performed TPO to quantify evolution of H<sub>2</sub>O in catalysts to elucidate the speciation of Mo-oxides

47 48

25 in H-ZSM-5, consistent with previous approaches by Iglesia et al. [22] Anchoring of Mooxides on zeolitic

49

50

<sup>2+</sup> dimer on double 26 BAS leads to desorption of H<sub>2</sub>O. Nominally (**Figure 2**), the formation of: (i) a

 $Mo_2O_5$ 

- 27 Al-atom sites yields one  $H_2O$  molecule (H/Mo = 1); (ii) a  $MoO_2^{2+}$  monomer on double Al-atom sites yields
- one  $H_2O$  molecule (H/Mo = 2); and (iii) a  $MoO_2OH^+$  monomer on a single Al-atom site yields no  $H_2O$

55 56 57

58 59

3 1 molecules (H/Mo = 0). Thus, calculating the atomic H/Mo ratios by  $H_2O$  quantification during TPO can 4 5 2 reveal structural information about the anchored Mo-oxides.

- 3 3.1.1. H<sub>2</sub>O evolution on Mo/H-ZSM-5 prepared by physical mixing (PM)
- 4 We investigated H<sub>2</sub>O evolution during TPO of physically mixed Mo/H-ZSM-5 (Mo/Z-PM in **Table**
- 1) using the temperature profile in **Table 2** for PM samples. **Figure S1 (a)** shows the H<sub>2</sub>O desorption

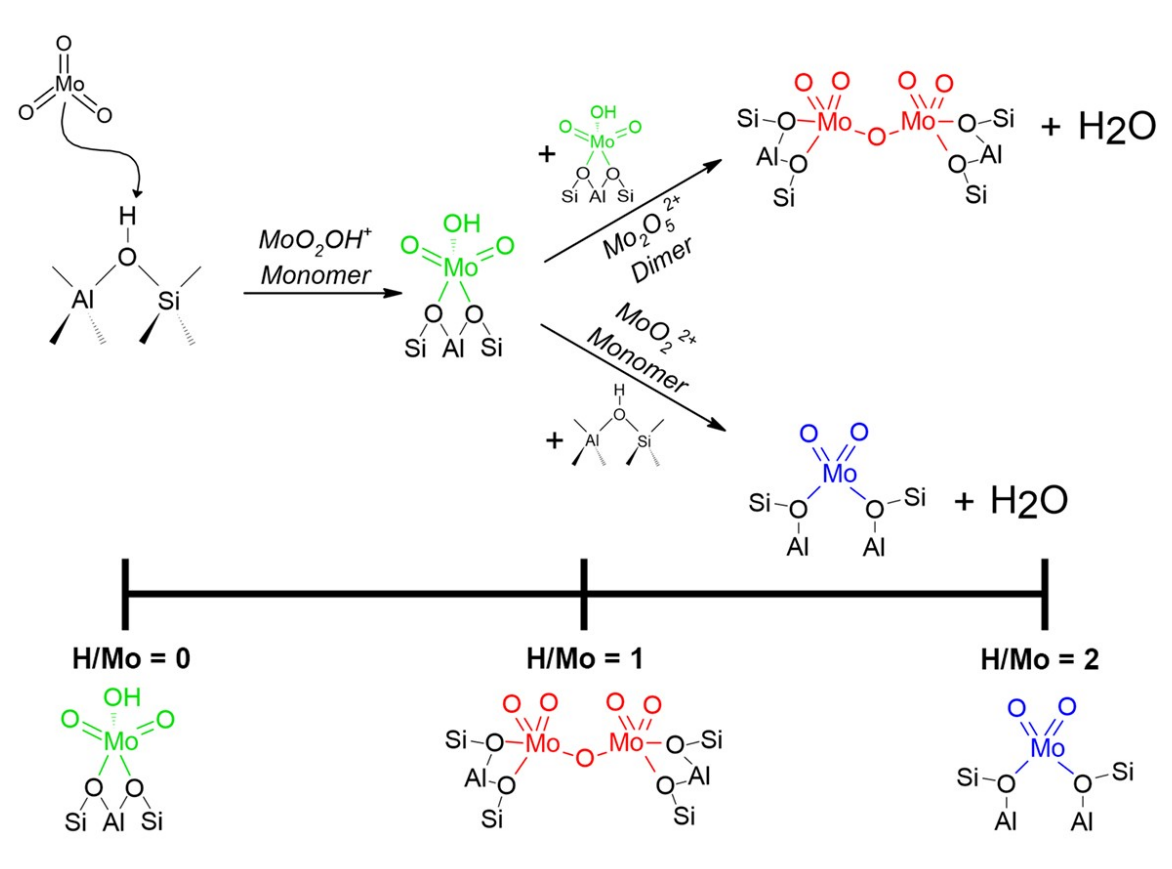


Figure 2. Mechanisms leading to different anchored Mo-oxide species, along with nominal H/Mo ratios from TPO.

ofi le of a  $\mathbf{M}$ o/Z-P M cat aly st over the ent ire te mp era tur e ran ge of TP O. Th e str on

6

pr

51 52

53 54

55 56

57

58

59 60 g H<sub>2</sub> O sig nal ob

43 44 d [22], 7 W hil e he ati ng fro m ~2 0 to 35 0 °C is attr ibu ted to des orp tio n of mo ist ure Asrep ort ed in lite rat ure

ser ve

h eat ing fro m 35 0 to 70 0 °C all ow S M οO 3 cry sta llit es to dis per se on the ze olit e's ext

8

46 47

9

eventually leading to migration of MoO<sub>x</sub> species into zeolite channels. Subsequently, they can exchange

52 53 54

51

55 56

57 58

59 60 ern al sur fac e,

48

49 10 onto zeolitic BAS to form anchored Mo-oxides depicted in **Figure 2**. The formation of H<sub>2</sub>O due to 50 11 anchoring is evidenced in TPO (**Figure S1 (a)**) by the distinct peak between 350 and 700 °C. Therefore, 12 analyses of desorbed H<sub>2</sub>O from metal oxide anchoring in PM samples were performed within this range.

13 **Figure 3 (a)** shows the H<sub>2</sub>O desorption rates above 350 °C during TPO of Mo/Z-PM (15) catalysts 14 with varying Mo loadings (Mo/Al = 0 – 0.45). H<sub>2</sub>O formed during TPO of bare H-ZSM-5 (Mo/Al = 0) at

Page 14 of 41

these elevated temperatures has been attributed to the condensation of two neighboring BAS in the presence of  $O_2$ , resulting in the formation of extraframework  $Al_2O_3$  (i.e., framework dealumination)<sup>[22]</sup>.

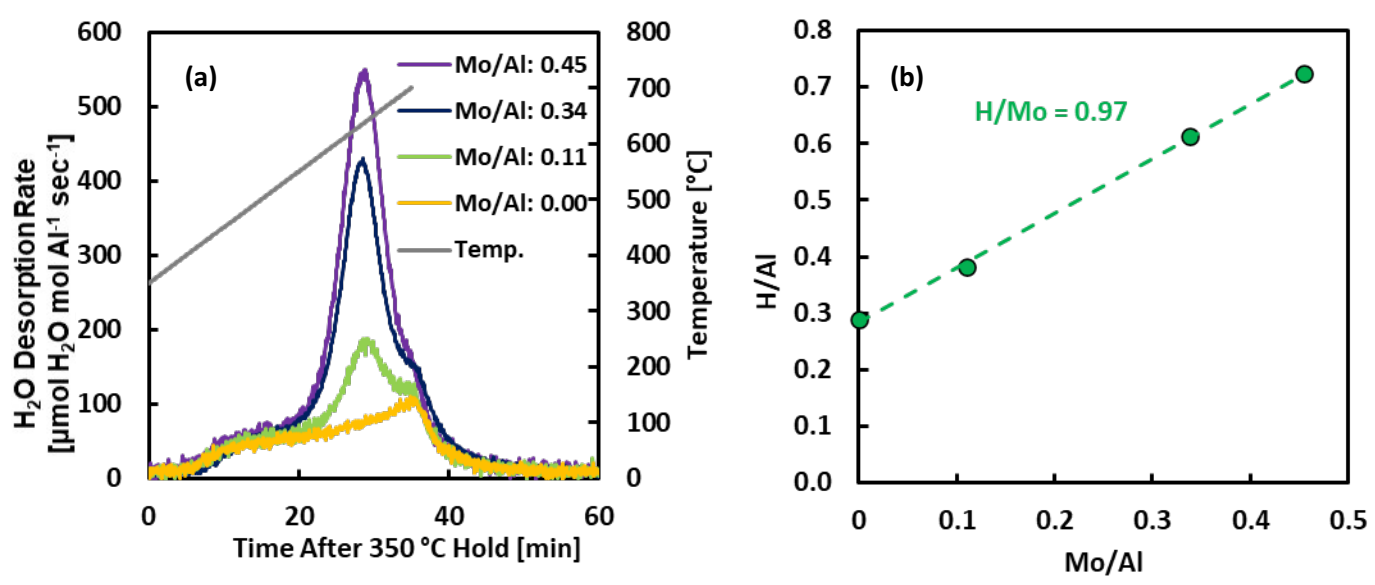


Figure 3. (a) Desorption rate of H<sub>2</sub>O per mol Al with varying Mo loadings in Mo/Z-PM (15) catalysts from 350 to 700 °C at 10.0 °C min<sup>-1</sup>. (0.3 g, 100 cm<sup>3</sup> min<sup>-1</sup>, 20% O<sub>2</sub>/Ar); integrated areas were calculated to quantify H/Al ratios. Solid gray line represents the PM temperature program as described in **Table 2**; (b) Ratio of H/Al from desorbed H<sub>2</sub>O during TPO of Mo/Z-PM (15) catalysts as a function of Mo loading.

- 3 The amount of H<sub>2</sub>O formed above 350 °C increases with Mo loading, with a peak H<sub>2</sub>O desorption rate at
- 4 630 °C. **Table 3** details the atomic ratios calculated from integration of the H<sub>2</sub>O desorption curves (H/Al)
- 5 for each Mo loading (Mo/Al) to determine the stoichiometry of Mo exchanging onto BAS (H/Mo). H<sub>2</sub>O
- 6 contributions from dealumination were accounted for by subtracting H/Al of the bare H-ZSM-5 from H/Al
- 7 in Mo/H-ZSM-5 catalysts (denoted as the H/Al<sub>F</sub> column in **Table 3** where Al<sub>F</sub> refers to framework Al)
- 8 assuming that the extent of dealumination is equal in both Mo-containing and bare H-ZSM-5. Plotting

51 52 53 the

5

6

7

0.

.2

1

2

3

2

.5

.6

.7

desorbed  $H_2O$  per Al site as a function of Mo/Al shows that approximately one proton is exchanged per 10 anchored Mo (H/Mo = 0.97) (**Figure 3 (b)**) which closely corresponds to the expected value if only 11 dimeric species,  $Mo_2O_5^{2+}$ , were formed (H/Mo = 1), suggesting that a prevalence of dimeric anchored 12 Mooxides exists within physically mixed Mo/H-ZSM-5 catalysts.

Page 15 of 41

### Similar measurements were performed on Mo/Z-PM catalysts using a lower acidity H-ZSM-5 support 8 (Si/Al = 40). Analysis of the corresponding $H_2O$ evolution curves (**Figure S2** and **Table S2**) between 350 °C and 700 °C in Mo/Z-PM (40) at the same Mo/Al ratios (0 - 0.45) yields a lower ratio of H/Mo = 0.77, 10 suggesting a decrease in the formation of the dimeric Mo-oxides. This is reasonable given that the + structures being near enough to form the dimer is decreased 11 probability of two anchored MoO<sub>2</sub>OH 12 support with fewer BAS. Table 3 H<sub>2</sub>O quantification from TPO of Mo/Z-PM (15) catalysts above 350 °C. <sup>a</sup> H/Al<sub>F</sub>

values were obtained by subtracting the H/Al of the bare H-ZSM-5 from the H/Al  $^b$  33 measured for each Mo-containing catalyst. H/Mo values were obtained by dividing 34 H/Al<sub>F</sub> by the corresponding Mo/Al ratio.

Catalyst	Nominal Mo loading [wt.%]	Nominal Mo/Al	H/Al	H/Al <sub>F</sub> <sup>a</sup>	H/Mo <sup>b</sup>
H-ZSM-5	0	0	0.29	0	-
1-Mo/Z-PM (15)	1	0.11	0.38	0.09	0.86
3-Mo/Z-PM (15)	3	0.34	0.61	0.32	0.96
4-Mo/Z-PM (15)	4	0.45	0.72	0.44	0.96

#### 3.1.2. H<sub>2</sub>O evolution on Mo/H-ZSM-5 prepared by incipient wetness impregnation (IWI)

We investigated  $H_2O$  evolution during TPO of Mo/H-ZSM-5 prepared by incipient wetness impregnation (Mo/Z-IWI from **Table 1**) using the temperature profile in **Table 2** for IWI samples. **Figure 8** 

- 4 S1 (b) shows the H<sub>2</sub>O desorption profile of a Mo/Z-IWI catalyst over the entire temperature range of TPO.
- 5 Similar to Mo/Z-PM in **Figure S1** (a), an initial intense H<sub>2</sub>O signal was observed attributed to moisture,
- followed by two more peaks at higher temperatures which we assign to H<sub>2</sub>O formed from Mo-oxide
- 7 anchoring. Thus, analyses of H<sub>2</sub>O evolution in IWI samples at different Mo loadings were performed
- 15 8 between 200 500 °C and 500 700 °C, as shown in **Figure 4**. Additionally, to account for H<sub>2</sub>O
- 17 9 contributions from the AHM precursor, we quantified H<sub>2</sub>O formed during TPO of pure AHM between
- 19 10 200 500 °C (Detailed in **Figure S1 (c)** and **Table S1**) and subtracted the corresponding amounts from
- 21 11 H/Al in Mo/H-ZSM-5 catalysts in this range (**Table 4**). A significant H<sub>2</sub>O signal remains in the samples
- 22 12 even after subtracting contributions from AHM, which we attribute to anchoring of Mo-oxides at much 23
- lower temperatures (~400 °C) than in Mo/Z-PM catalysts (~650 °C).

51

9

11

13

16

18

20

25

57 58

59

56

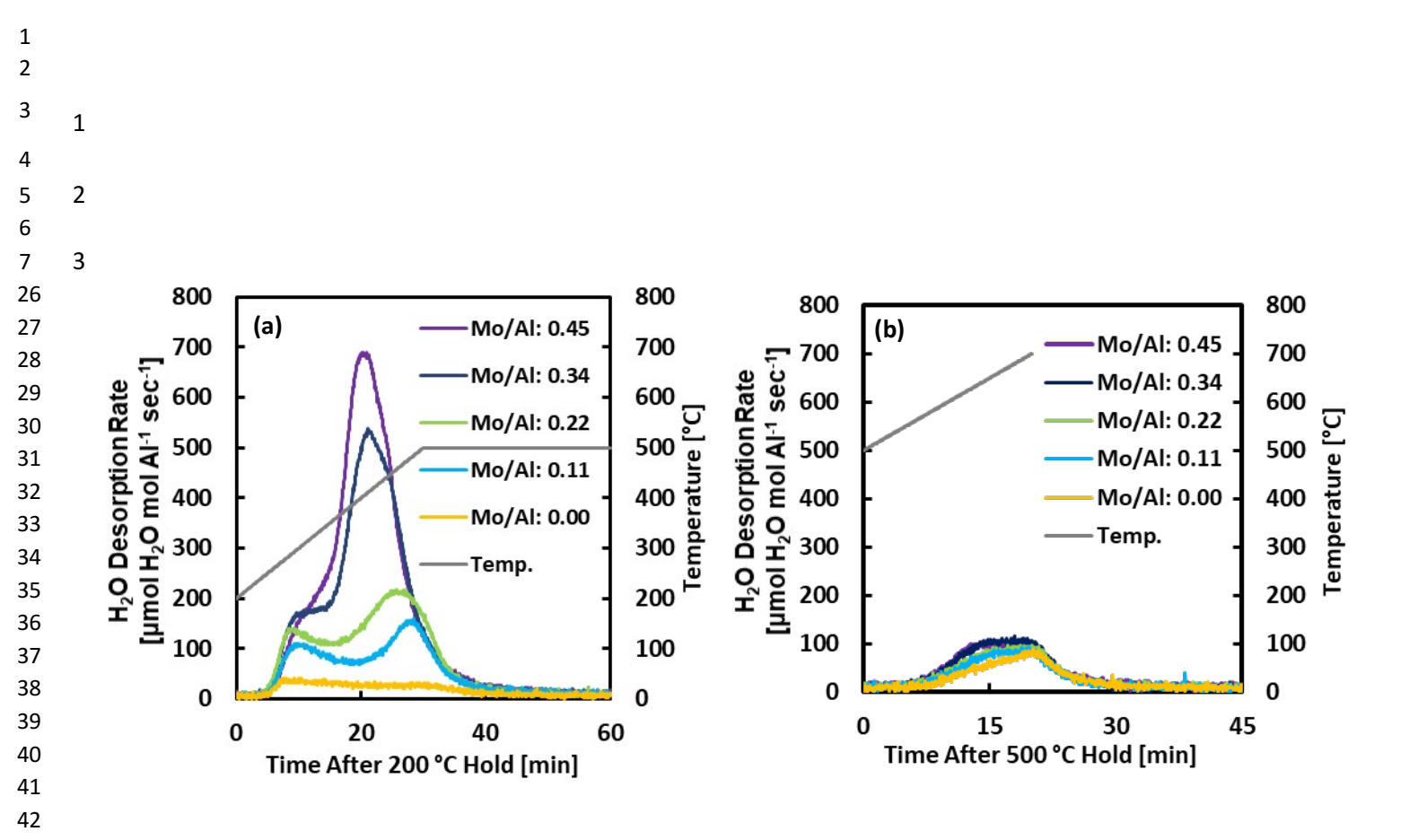


Figure 4. (a) Desorption rate of H<sub>2</sub>O per mol Al with varying Mo loadings of Mo/Z-IWI (15) from 200 to 500 °C at 10.0 °C min<sup>-1</sup>. (b) Desorption rate of H<sub>2</sub>O per mole of Al with varying Mo loadings of Mo/Z-IWI (15) from 500 to 700 °C at 10.0 °C min<sup>-1</sup>. Solid gray line represents the corresponding temperature program as 47 described in **Table** 

Anchoring at a lower temperature with IWI catalysts is feasible if we consider that the chemistry of 49 14 15 the Mo precursor, ammonium heptamolybdate tetrahydrate (AHM, (NH<sub>4</sub>)<sub>6</sub>Mo<sub>7</sub>O<sub>24</sub>.4H<sub>2</sub>O) in aqueous 16 solution differs from MoO<sub>x</sub> species originating from MoO<sub>3</sub> crystallites at higher temperatures, as is the 17 case with Mo/Z-PM catalysts. According to Barath et al. [54], an ionic equilibrium (Mo<sub>7</sub>O<sub>24</sub><sup>6-</sup> + 4H<sub>2</sub>O  $\leftrightarrow$ 

43

44

45

46

48

50

59 60

7MoO<sub>4</sub><sup>2-</sup> + 8H<sup>+</sup>) occurs when AHM is dissolved in water. We postulate that sufficiently small, aqueous 18 Page 17 of 41

- MoO<sub>4</sub><sup>2-</sup> ions are able to diffuse into the zeolite channels during IWI and remain there after drying, thereby
- eliminating the need to reach elevated temperatures required for MoO<sub>3</sub> sublimation and migration when
- using the PM method. Thus, IWI would enable Mo anchoring between 200 500 °C. H<sub>2</sub>O quantification
- 4 of catalysts within this range (**Table 4**) and plotting the corresponding H/Al as a function of Mo loading
- (**Figure 5**) yields H/Mo = 1.6. This non-integer value suggests not only a difference in Mo-oxide
  - speciation compared to PM catalysts (perhaps some presence of MoO<sub>2</sub><sup>2+</sup> monomers), but also species
  - heterogeneity in IWI catalysts.
- <sup>a</sup> Total H/AI from 200-500
- Table <sup>b</sup> H/Al contributions from AHM from 200 500 °C at each Mo/Al. 4. H<sub>2</sub>O quantification from TPO of Mo/Z-IWI (15) catalysts from<sup>c</sup> (H/Al 200) <sub>1</sub>- values were obtained by subtracting (H/Al) 500 °C & 500 - 700 °C. AHM from
- °C. d (H/Al<sub>F</sub>)<sub>1</sub> values were obtained by subtracting (H/Al)<sub>1</sub> of bare H-ZSM-5 from (H/Al)<sub>1</sub> of the Mo-containing catalysts from 18 (H/AI). <sup>e</sup> (H/Mo)<sub>1</sub> values were obtained by dividing (H/AI<sub>F</sub>)<sub>1</sub> by the corresponding Mo/AI ratio. <sup>f</sup> Total H/AI from 500 – 700 19 200°C. – 500 °C. g (H/Al<sub>F</sub>)<sub>2</sub> values were obtained by subtracting (H/Al)<sub>2</sub> of bare H-ZSM-5 from that of Mo-containing catalyst from 500 – 700 20 °C. h (H/Mo)2 values were obtained by dividing (H/AI<sub>F</sub>)2 by the corresponding Mo/AI ratio.

	Catalyst	Mo loading [wt.%]	Nominal Mo/Al	H/Al <sup>a</sup>	(H/Al)ahmb	(H/Al) <sub>1</sub> <sup>c</sup>	$(H/Al_F)_1^d$	$(H/Mo)_1^e$	(H/Al) <sub>2</sub> <sup>f</sup>	(H/Al <sub>F</sub> ) <sub>2</sub> <sup>g</sup>	(H/Mo) <sub>2</sub> <sup>e</sup>
-	H-ZSM-5	0	0	0.09	0	0.09	0	=	0.15	0	-
	1-Mo/Z-IWI (15)	1	0.11	0.30	0.05	0.25	0.16	1.46	0.20	0.05	0.46
	2-Mo/Z-IWI (15)	2	0.22	0.50	0.09	0.41	0.32	1.43	0.17	0.02	0.11
	3-Mo/Z-IWI (15)	3	0.34	0.85	0.14	0.71	0.62	1.82	0.21	0.06	0.19
_	4-Mo/Z-IWI (15)	4	0.45	0.93	0.19	0.75	0.66	1.45	0.20	0.06	0.12

Quantification of desorbed H<sub>2</sub>O between 500 – 700 °C shows little H<sub>2</sub>O formation across Mo loadings.

2		
3	1	
4		
5	2	
6	2	
7 35	3 10	XAS analysis of Mo/Z-IWI (15) catalysts, shown in the next section, shows no appreciable change
33		local
36		
37 : 38	11	Mo structure within this temperature range, suggesting that most of the Mo-oxide anchoring occurs during
39	12	the lower temperature range of $200-500^{\circ}\text{C}$ . We surmise that $H_2O$ contributions between $500-700^{\circ}\text{C}$
40 41	13	can be attributed to either dealumination or formation of minor amounts of aluminum molybdate. X-ray
42 : 43	14	diffraction of Mo/H-ZSM-5 catalysts after TPO was also performed to ensure Mo dispersion into zeolite
44 : 45	15	channels after TPO. The diffraction patterns shown in Figure S3 indicate that, other than diffraction peaks
46	16	from H-ZSM-5, no other peaks from any Mo-containing phases were detected in the catalysts. This
47 48	17	suggests that the Mo species did not form any crystalline phases on the zeolite's external surface.
49 : 50	18	The quantitative TPO results point to a difference in the distribution of Mo-oxide species as a function
	19 (	of the synthesis method. The slopes of the H/Al versus Mo/Al plots obtained from H <sub>2</sub> O quantification 20 yield
	nor	n-integer values of H/Mo that vary depending on synthesis method, implying coexistence of 21 distinct Mo-
	oxi	de species of different distributions. Physically mixed catalysts (H/Mo = 0.97) suggest a
	22	prevalence of dimeric $Mo_2O_5^{2+}$ , whereas IWI catalysts (H/Mo = 1.6) suggest a distribution of Mo-oxide Page 18 of 41

species, with potentially some presence of monomeric  $MoO_2^{2+}$ . We point out that while the PM synthesis method involves a solid-state introduction of  $MoO_x$  into H-ZSM-5 using the  $MoO_3$  solid precursor, in the

IWI method the Mo precursor, (NH<sub>4</sub>)<sub>6</sub>Mo<sub>7</sub>O<sub>24</sub>4H<sub>2</sub>O, is dissolved in a liquid state prior to calcination. We

4 posit that this synthesis-dependent difference in speciation is caused by the different chemistries involved

5 in the different mechanisms for migration of the Mo species inside the zeolite channels as a consequence

of the different speciation of the starting Mo precursors (MoO<sub>3</sub> versus (Mo<sub>7</sub>O<sub>24</sub>)<sup>6-</sup>). To test this hypothesis,

7 we performed operando XAS measurements as described in the following section.

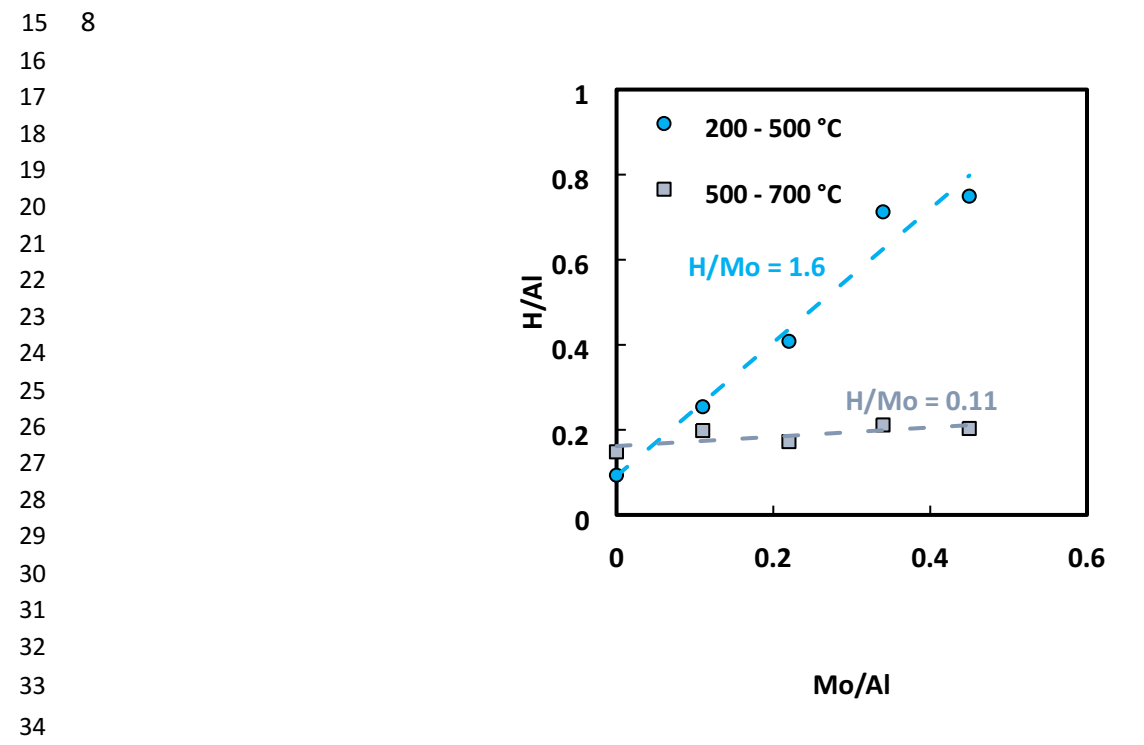


Figure 5. Ratio of H/Al from desorbed  $H_2O$  during TPO of Mo/Z-IWI (15) as a function of Mo loading. Circle points 36 correspond to  $H_2O$  formed between 200 – 500 °C, square points correspond to  $H_2O$  formed between 500 – 700 °C.

## Chemistry of Materials

# 3.2. Monitoring local electronic structure of Mo species during calcination by operando XANES

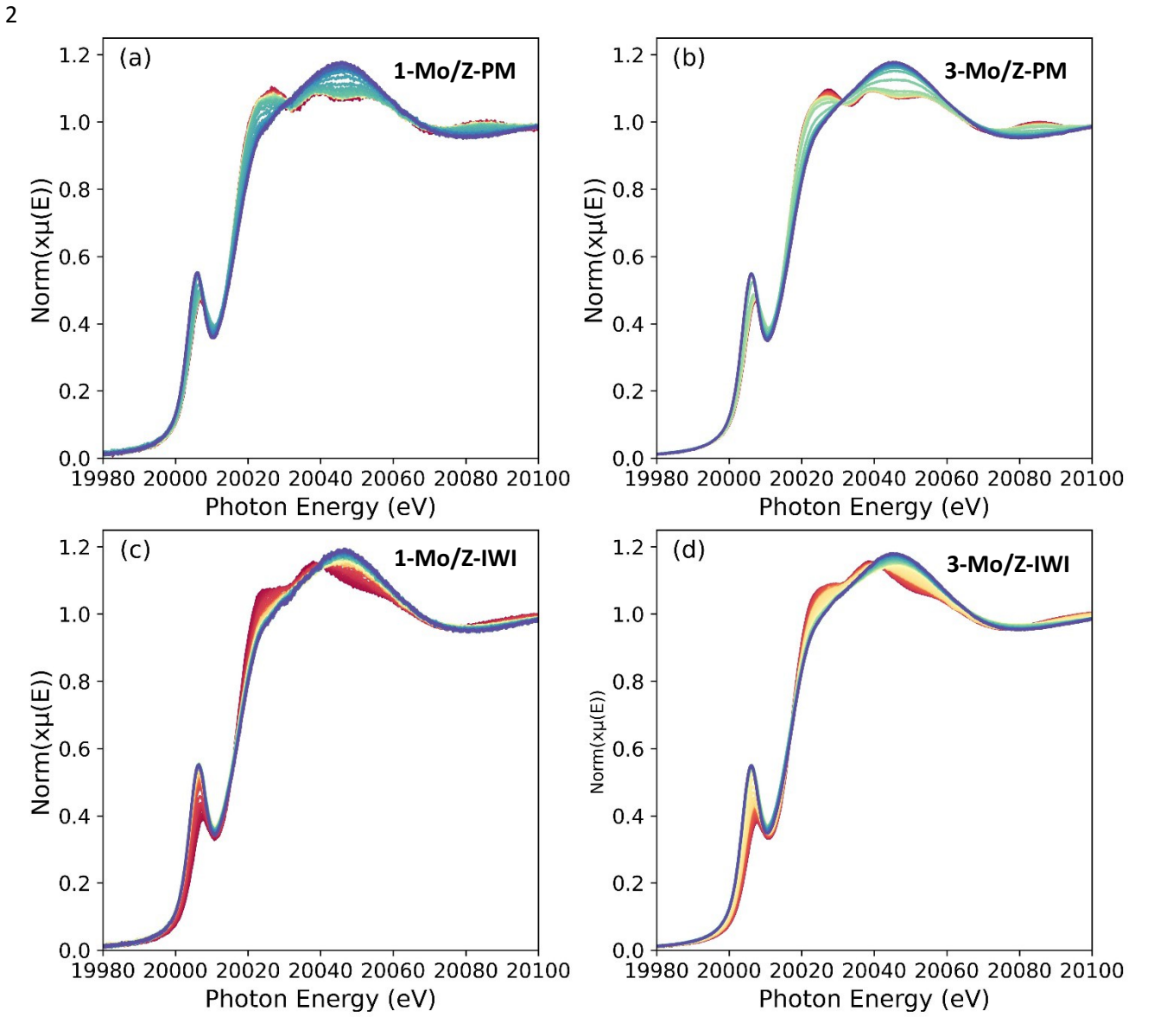


Figure 6. Operando Mo K -edge XANES spectra of pre -catalysts undergoing TPO employing the corresponding temperature profiles for PM and IWI catalysts as shown in **Table 2**. (a) 1-Mo/Z-PM; (b) 3-Mo/Z-PM; (c) 1-Mo/Z-IWI; (d) 3-Mo/Z-IWI. Si/AI = 15 in all catalysts. C olor gradient from red to blue corresponds to a temperature change from room temperature, approximately 20 °C, to 700 °C, respectively.

- To analyze possible differences in the Mo-oxide local structures from different anchoring pathways
- 4 associated with differently synthesized catalysts, we performed operando Mo K-edge XANES
- 5 measurements of the catalysts during TPO. **Figure 6** shows the evolution of 1 & 3-Mo/Z-PM (15) and 1

1 2	
3	1
4	
5	2
6	
7	3

- 6 & 3-Mo/Z-IWI (15) catalysts using the corresponding TPO temperature profiles shown in **Table 2**. The 7 pre-edge feature of both sets of catalysts grows increasingly pronounced with temperature (with a final
- 8 pre-edge energy at 20,005 eV), indicating a change in the local geometry of the Mo structure to a more

tetrahedral character. The initial XANES spectra of the four samples pre-TPO, **Figure S4 (a)**, show that the starting Mo species are dependent on the Mo precursor used in synthesis, MoO<sub>3</sub> or AHM. By the end of the TPO experiments however, XANES spectra detailed in **Figure S4 (b)** show that the Mo species 8

- 4 exhibit the same average electronic structure across the four samples, regardless of synthesis technique
- 10 5 and Mo loading.

11 12

15

18

25

27

32

- Principal component analysis (PCA) and multivariate curve resolution-alternating least squares
- 14 7 algorithm (MCR-ALS) were used to identify the number of dominant spectral signatures that make up the
- 16 8 XANES data during the TPO. These a priori analysis methods identify how spectra evolve over
- 9 time/temperature, identify similar spectral features in datasets, and can be used to identify potentially
- hidden or minority features. To best resolve subtle differences in the four datasets, all XANES spectra of
- 21 11 the four samples were analyzed simultaneously. The scree plot of the PCA (Figure S5 (a)) showed that
- 22 12 all four XANES spectra can be described with three components, constituting 99.999% of all spectra in 23
- the dataset. The first five eigenspectra generated in the PCA (**Figure S5 (b)**) show that the predominant
- spectral differences occur around the pre-edge peak and white line, which is expected because the largest
- 28 15 changes observed in the XANES spectra (Figure 6) occur in this region. When comparing how the first
- 29 16 three eigenspectra (i.e., components) are correlated as a function of XANES spectra during the TPO, the 30
- 31 17 score plot in **Figure S5 (c)** shows that the four samples start in two distinct regions with the final spectra
- 33 18 being clustered in a third region. The initial two groupings, representing the XANES spectra
- 34 19 corresponding to the initial as-prepared samples (**Figure S5 (c)**) differentiate the samples by the method 35
- of synthesis (physical mixing with MoO<sub>3</sub> or incipient wetness impregnation with AHM). This matches

52 53

53 54

51

55 56

57 58

2		
3 1		
4		
5 <b>2</b> 6		
7 3		
37		
38 21 39	the grouping observed in the initial XANES spectra of each sample (Figure S4 (a)). The clustering of the	he
40 22	eigenspectral components at the end of the TPO for the four samples show that the end states are near	
41 23 42	identical (Figure S5 (c)), indicating that the Mo species in both PM- and IWI-prepared catalysts appear	
43 24 44	to converge to a distinct final state over the course of TPO, matching the same observation in the end st	ate
45 <b>25</b> 46	XANES spectra, Figure S4 (b). While PCA can deconvolute the spectra into their major components	,
	interpretation of the eigenspectra is difficult, leading to use of the approximate deconvolution results from	n
48 27 50 28	the MCR-ALS analysis guided by PCA results to determine speciation and species evolution during the TPO.	19
29	A three-component MCR-ALS spectral deconvolution was performed based upon three principal	
30	components from the knee of the PCA scree plot. The eigenspectra from the MCR-ALS deconvolution	on
31	are plotted in <b>Figure S6</b> and will be discussed further below. The concentration of each eigenspectru in	ım
Page 2		
1 2		
3 1 4	each XANES spectrum, along with the simultaneous evolved $H_2O$ (m/z = 18) signal from the mass	
5 <b>2</b>	spectrometer, is plotted as a function of temperature in Figure 7. PM- and IWI-prepared catalysts initia	lly
7 3 8	have different eigenspectral compositions at the start of the TPO based on synthesis method, consistent	ıt
9 4	with the as-prepared XANES spectra and PCA analysis. As the temperature increases to 700 °C, all four	
51 52 53 54 55 56		
58		
59		50

## Chemistry of Materials

10 11	5	samples transition from their initial eigenspectral compositions to a uniform final eigenspectral
12 13	6	composition. This uniform composition is consistent with the XANES spectra collected at 700 °C and the
14 15	7	composition of PCA components for the corresponding spectra.
16	8	The eigenspectra generated in the MCR-ALS analysis were normalized and compared to XANES
17 18	9	spectra of bulk Mo compounds ( <b>Figure S6</b> ). Eigenspectrum #1, the component that represented the final
19 í	10	state post-TPO for all samples, did not appear to match any known oxidic Mo compound we referenced.
21	11	This may be interpreted as heterogeneity in the structure of the anchored Mo-oxides, seeing as multiple
22 23	12	different spectra could contribute to produce a unique spectrum. Eigenspectrum #2, the dominant
24 í 25	13	component of the as-prepared physically mixed samples, is a close match to XANES spectra of MoO <sub>3</sub> .
26 í	14	Finally, eigenspectrum #3, the dominant component of the as-prepared incipient wetness impregnated
28	15	samples, is a close match to the XANES spectra of AHM. The similarities of the two eigenspectra, and a
29 30	16	priori analysis result, to the XANES spectra of the appropriate precursors for each synthesis methods (PM
31 : 32	17	or IWI), along with a unique third eigenspectrum that represents the common end state supports that the
33	18	three-component analysis is sufficient to describe the evolution of the Mo in each pre-catalyst.
34 35	19	During TPO, the temperature at which the conversion from the initial eigenspectral composition to the
36 2 37	20	final composition occurs is different based on the synthesis method/precursor of the catalyst as shown in
38 2 39	21	Figure 7. Mo/Z-PM (15) catalysts show that significant change in the composition of XANES spectra
40	22	occurs between 400 – 500 °C ( <b>Figure 7 (a) &amp; (b)</b> ), where the final state component (eigenspectrum #1)
41 42	23	increases as the MoO <sub>3</sub> -like component (eigenspectrum #2) decays. Here, we can see that the initial MoO <sub>3</sub>
43 2 44	24	precursor requires elevated temperatures to decompose before mobilizing into zeolite channels and
45 2	25	exchanging onto zeolitic BAS, consistent with reports from literature <sup>[22]</sup> . This change is independent from
51 52 53 54 55 56 57 58		
59		ACS Paragan Plus Environment
60		ACS Paragon Plus Environment

1 2			
3	1		
4			
5	2		
6			
7	3		
46 47	26	tl	he removal of adsorbed water in the zeolite (between 20 - 200 °C) and simultaneously corresponds to the
48 49	27	' e	evolution of water due to anchoring (above 400 °C) as determined in the quantitative H <sub>2</sub> O evolution
	28	stu	dies (see Figure 3). In contrast, IWI-prepared catalysts change from their initial states to the final states 29
	be	twe	een $100 - 300$ °C, with the 1-Mo/Z-IWI (15) sample being almost fully converted to its final state by
	30		the time the adsorbed water is completely removed from the zeolite (Figure 7 (c)). For 3-Mo/Z-IWI (15),
		31	we see a slight rise in the MoO <sub>3</sub> -like component with the reduction of the initial AHM-like component
			Page 22 of 4
			(eigenspectrum #3) before also disappearing at elevated temperatures (Figure 7 (d)), consistent with
de	con	npc	osition of the heptamolybdate species into smaller Mo-oxide species and subsequent dispersion of these
Mo	0-0	xid	les above 300 °C <sup>[55]</sup> . However, because the conversion into the final state begins at a lower 8
9	4	t to	emperature prior to noticeable MoO3 eigenspectral character emergence, we interpret this as further
10 11	5	e e	evidence that IWI allows aqueous MoO <sub>4</sub> <sup>2-</sup> ions to diffuse into and remain within zeolitic channels during

temperature, coinciding with the initial removal of moisture from the zeolite, whereas Mo in the PM
catalysts are mobile only at higher temperatures, well after the last detected moisture-attributed water was
removed. This analysis of operando XANES data is not sensitive enough to distinguish the subtle
structural differences between the various Mo-oxide species formed after TPO as a function of synthesis
method and Mo loading, but it does underpin the clear difference in the temperature at which the different
Mo precursors mobilize and anchor on zeolitic BAS.

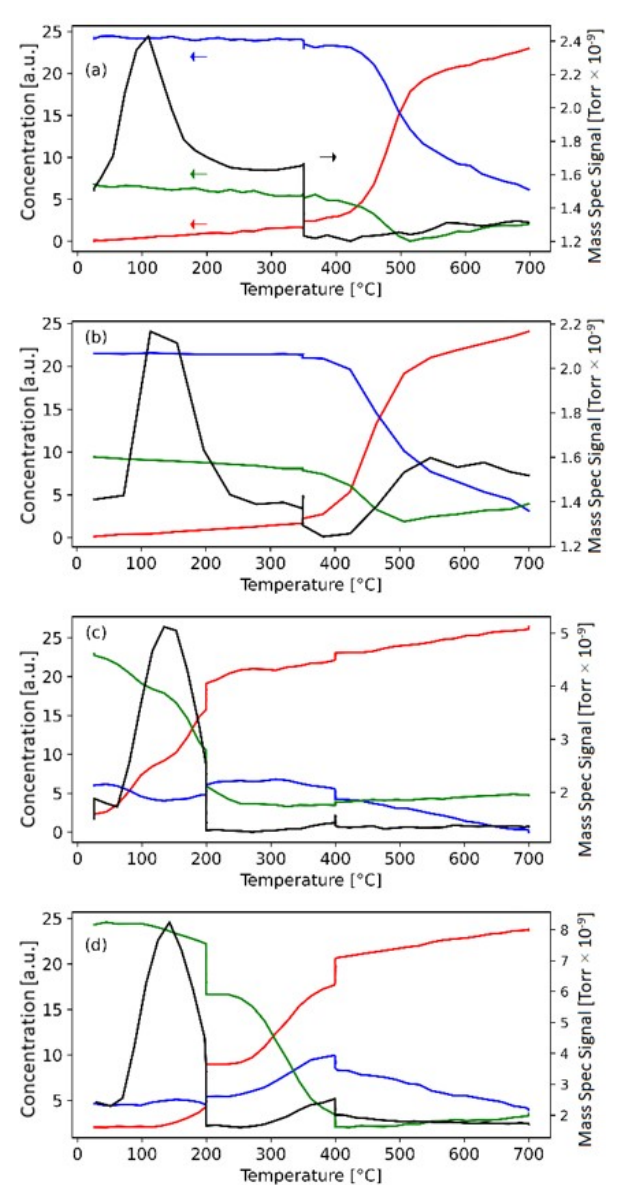


Figure 7. Eigenspectra concentrations (red, blue, green) of XANES spectra recorded at the Mo K-edge during the TPO and the mass spectrometer water signal (m/z = 18), black, as a function of temperature for a) 1-Mo/Z-PM (15), b) 3-Mo/Z-PM (15), c) 1-Mo/Z-IWI (15), and d) 3-Mo/Z-IWI (15). Red line: concentration of eigenspectrum #1 (post-TPO-like), Blue line: concentration of eigenspectrum #2 (MoO<sub>3</sub>-like), Green line: concentration of eigenspectrum #3 (AHM-like).

## Chemistry of Materials

1 2 3 4 5 6 7 45 46 47 48 49 50		While quantitative H <sub>2</sub> O evolution studies elucidate the varying stoichiometric interactions of Mo with 3 colitic BAS associated with the anchoring process and operando TPO XANES experiments elucidate the evolution of the Mo species, these data do not provide direct structural information due to lack of
		Page 24 of 41 sensitivity (XANES) or ability to determine structure (mass balances from TPO). Therefore, we employ
DF	Γ-as	ssisted EXAFS analysis (QuantEXAFS <sup>[40]</sup> ) to understand the local coordination environment of Mo atom(s).
Nex	kt, v	we discuss the DFT calculations that were used to atomistically characterize and assess the 8
9	4	viability of these various motifs. The structures predicted through these calculations form the database of
10 11	5	62 structures which we use for comparison with our experimentally measured EXAFS spectra through
12 13	6	QuantEXAFS analysis.
14 15	7	3.3. DFT Calculations of Anchored Mo-oxide Species
16	8	Discussion on Mo-oxide species' structures within H-ZSM-5 has been the subject of many theoretical
17 18	9	papers; however, most studies have focused on cluster models <sup>[18, 29,56, 57]</sup> rather than studying the anchored
51 52 53 54 55 56 57 58		

19 10 Mo-oxides within bulk H-ZSM-5. In this work, various MoO<sub>x</sub> motifs were studied within the fully periodic 20

21 11 H-ZSM-5 unit cell (with lattice constants a = 20.14 Å, b = 20.39 Å, and c = 13.53 Å; 0.33%, 2.34%, and

22 12 0.85% larger than experiment<sup>[48, 58]</sup>). We have considered a range of Al-substituted T-sites as well as 23

qualitative motifs (monomeric and dimeric MoO<sub>x</sub> species) in this analysis. MoO<sub>x</sub> nanostructures anchored

on a single (a) and double Al-atom site (b,c) are shown in Figure 8.

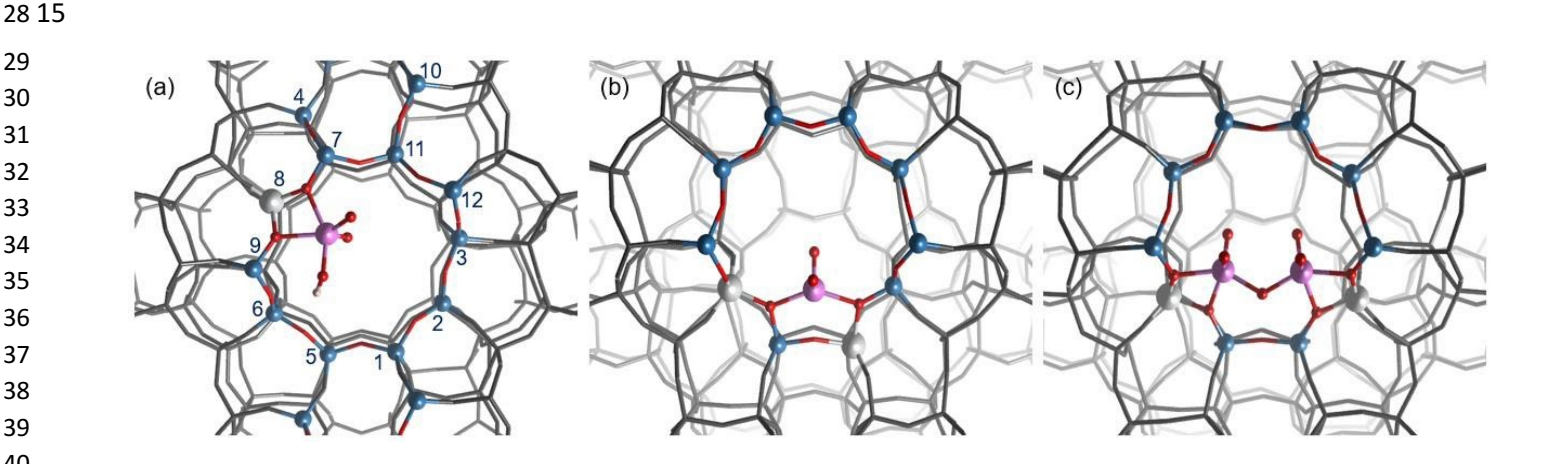


Figure 8. Overview of qualitatively distinct catalyst precursor structural motifs: (a) Isolated MoO₂OH<sup>+</sup> monomer structure anchored on a single Al-atom framework site. T-sites 1-12 are labeled with corresponding numbers for reference. (b) Isolated MoO<sub>2</sub><sup>2+</sup> monomer structure anchored on double (next-nearest neighbor, NNN) Al-atom <sup>2+</sup> framework site. (c) Isolated Mo<sub>2</sub>O<sub>5</sub> dimer anchored on double (next-next-nearest neighbor, NNNN) Al-atom 47 framework site. Color scheme: silicon (blue), oxygen (red), aluminum (silver), molybdenum (magenta), hydrogen 48 (white), nonspecific framework (grey).

49 16 50

43

44

45

46

24 13 25

26 14 27

29

> 17 18

#### 3.3.1. Structures of Mo-oxides in H-ZSM-5

• MoO<sub>2</sub>OH<sup>+</sup> structure anchored on single Al-atom framework site 19

Page 25 of 41

56 57 58

59

2		
3	1	
4		
5	2	
o 7	3	
L		
2		
3 1	The structure of a geometrically optimized Mo mono	omer anchored on a single Al-atom framework
5	2 site (T-site 8) is shown in <b>Figure 8 (a)</b> . In the MoO <sub>2</sub> OH <sup>+</sup> n	nonomer structure, Mo is bidentately coordinated
7	3 to the framework through two framework oxygen atoms	s (Mo-O <sub>F</sub> bond length 2.16 – 2.35 Å, O-Mo-O
9	4 angle $67 - 69^{\circ}$ among structures studied). These structures	also feature two terminal Mo=O double bonds
10 12	` '	These results agree with previous literature 11 reports by Podkolzin and co-workers <sup>[18, 26]</sup> .
13		monomers have focused on anchoring either on e T-site
14		Previous literature reports on MoO <sub>2</sub> OH
15	5 [5,	<sup>18, 22, 23, 25, 26, 29, 56]</sup> , noting that the latter leads to
16	6 8	substituted by the Al atom or on external Si om sites
17	an as	the formation of a less stable (more weakly achored) monomer. In this work, we also sessed the
l8 19		10 viability of MoO <sub>2</sub> OH <sup>+</sup>
LJ		anchored at T-sites distant from the Al-substituted T-sites. In this outlook, all
20	0	<sup>+</sup> monomer anchoring sites. Our
- 4		
52	2	
51 52 53 54 55 56 57 58	3	
54	4	
55 56	5	
50 57	o 7	
58	8	
59		58

27 direct Mo-O<sub>F</sub>-Al coordination, the cationic character of the anchored Mo-oxide stabilizes the charge

50 28

imbalance. In motifs where the MoO<sub>2</sub>OH<sup>+</sup> anchors in a way that does not share a direct Mo-O<sub>F</sub>-Al coordination, the hydroxyl group of MoO<sub>2</sub>OH<sup>+</sup> points toward one of the Brønsted basic oxygen sites in the framework coordinated to the Al<sup>3+</sup> cation.

• MoO<sub>2</sub><sup>2+</sup> structure anchored on double Al-atom framework site

1 2 3 1 2 5 3 Page 26 of 41 On a site with two proximal acidic protons charge-compensating the net negative charge resulting from two framework Al<sup>3+</sup> cations, the MoO<sub>x</sub> stoichiometry of an anchoring monomer should be MoO<sub>2</sub><sup>2+</sup>. This MoO<sub>2</sub><sup>2+</sup> motif is shown in **Figure 8 (b)**. Because of Löwenstein's rule on Al siting and Al-Al distance <sup>2+</sup>, the only viable double Al-atom sites in the 10-member ring are NNN 8 constraints for anchoring MoO<sub>2</sub> and NNNN arrangements. Examples of these structures are shown in 10 Figure S7. In each of the eight 11 MoO<sub>2</sub><sup>2+</sup> structures, the Mo atom is roughly tetrahedrally coordinated, with two terminal Mo=O bonds 6 12 13 (length 1.70 Å) and a O=Mo=O bond angle of 106 – 107°. On the Al-O-(Si-O)<sub>2</sub>-Al (NNNN) anchoring 7 14 15 site, Mo is bidentately anchored to two framework oxygen atoms (Mo-O<sub>F</sub>) with bond distances of 2.07 – 16 2.10 Å and O<sub>F</sub>-Mo-O<sub>F</sub> angles of 135.4 – 135.8°. Comparing the Al-O-(Si-O)-Al-coordinated (NNN) 18 17 structures to the NNNN-coordinated structures, the distance between Mo and framework oxygen (Mo-19 10 20 21 11  $O_F$ ), and the bond angle slightly increased to 2.10 - 2.14 Å and  $140.1 - 140.5^{\circ}$ , respectively. This 12 observation could be attributed to the Mo monomer being more symmetrical when anchored at NNNN 22 23 sites and acidity being more potent<sup>[29]</sup>. The calculated geometries for MoO<sub>2</sub><sup>2+</sup>-7-11 (Al 8,12) agree with 24 13 25 51

52 29

## Chemistry of Materials

2		
3 .	1	
4	-	
	2	
6	3	
7 3	5	previous studies <sup>[18, 26]</sup> . For the MoO <sub>2</sub> <sup>2+</sup> -9-9 (Al 6,9) structure, the Mo-O <sub>F</sub> bond length of 2.10 Å is shorter
27		[29]. In comparison with experimental data on
28		than the 2.12, 2.37 Å reported in other DFT studies
29		16 comparable motifs in the literature <sup>[28]</sup> (Mo-O <sub>F</sub> : 1.85 Å and Mo=O: 1.69 Å), the Mo-O <sub>F</sub> bond lengths in
30 31 17 32	our models (2.07 – 2.14 Å) are consider	ably larger, but the Mo=O bond length (1.70 Å) agrees well. It is
33 1	8 expected that bond lengths of the function	al employed in this work will generally lead to slightly longer
34 19 35	9 bond lengths relative to experiment, althou	ugh often not by more than a handful of percent ( $\sim 2-4\%$ ) so
36 20 37	we find reasonable but not exceptional a	greement between our structures and experimental measurements
38 21 39	attributed to this motif. Summarized stru	actural details for the MoO <sub>2</sub> <sup>2+</sup> species in this work are provided in
40 2	2 Table S7.	
41 2	• Mo <sub>2</sub> O <sub>5</sub> <sup>2+</sup> structure anchored on double A	l-atom framework site 42
43 <b>2</b> 4 45	25	ies of a range of Mo <sub>2</sub> O <sub>5</sub> <sup>2+</sup> dimers anchored on different T44 sites inside straight and sinusoidal channels of H-ZSM-5, we dered all of the pairs of Al-substituted
46 47	<sup>2+</sup> mo 26	onomers plus additional sites to further represent the diversity of T-sites used in our study of MoO <sub>2</sub>
51 52 53 54 55 56		
58		
59 60		ACS Paragon Plus Environment

50 28 illustrated in **Figure S8**. Geometric descriptors for the 12 Mo dimer structures studied are reported in **Table S8**. The Mo dimers we observe are consistent with those reported by Bao and co-workers<sup>[29]</sup>, wherein the Mo atoms are each bidentately coordinated to two framework oxygens (Mo-O<sub>F</sub>), and the MoO-Mo bridge forms an obtuse angle pointed toward the channel center. This motif is qualitatively distinct

Page 27 of 41

1 2		
3	1	from the proposed structure by Iglesia and co-workers <sup>[25]</sup> , where each Mo atom connects with one
5	2	framework oxygen atom and the Mo-O-Mo bridge's obtuse angle instead points toward the channel wall.
7		3 This qualitative discrepancy between the predicted Mo <sub>2</sub> O <sub>5</sub> <sup>2+</sup> species and experimentally determined
8 9		[29]. Each Mo in this dimer 4 published structure is consistent with the observations of Bao and co-workers
10		5 motif is qualitatively trigonal bipyramidal in its coordination and the overall structure is roughly
11		
12		6 sy
		m
		me tric
		wit
51 52 2	9	
<sup>53</sup> 3	0	
54 5	5	
31 56		
57		
58		

## Chemistry of Materials

an O-Mo Mo **-**O dih edr al an gle of 1.5 26. 4°. Th e obt ain ed Mo  $O_{\mathsf{F}}$ bo nd len gth

h

59 60 64

s of 2.1 0

[25],

5 Å for all of the mo tifs , in ge ner al, are lon ger tha n the ex per im ent all y rep ort ed val ue of 1.7  $8\,\text{\AA}$ 

7

2.3

[29]

8

b ut in

go

52 29

51

15

16

<sup>53</sup> 30

54 55

31

56

57

58

59 60

ACS Paragon Plus Environment

## Chemistry of Materials

3

7

odagr ee me nt wit h the qu alit ati vel y si mil ar pre vio usl y pu bli she d DF Тopt imi zed str uct ure

51525354555657

58 59

9 F our ter mi nal Mo =0bo nds are eac h 1.7 1 -1.7 2Å lon g, in go od agr ee me nt wit

18 19

51 52 29

<sup>53</sup> 30

54 55

31

56

57

58

59 60

ACS Paragon Plus Environment

10

O-Mo bridge is 1.87 - 1.94 Å,

h bot h ex per im ent [25] an d previous DFT studies<sup>[29]</sup>. The obtained Mo-O bond distance in the Mo-

1 2				
3	1			
4	_			
5	2			
6 7	3			
20 21			[25], but which agrees well with the state of 1.84 Å	
22			bond distance of the DFT calculations (1.91 Å) <sup>l</sup> calculated Mo-Mo distances in o	<sup>29</sup> ]. The
23			1 1 1 1 1 1 1 1 1 1 1 1 1 1 1 1 1 1 1 1	8 \ 1
<ul><li>24</li><li>26</li><li>27</li></ul>		.33 - 3.54 Å, are smaller than the previous experimental studies agree well with the theoretical studies by Zhou et al. <sup>[29]</sup> (3.57)	` `	
	15	optimized geometry varies from $2.98 - 3.63$ Å; this longer Mo-	-Al distance (one Al-Mo distance is	~3 Å
31 32	17	and the other is $\sim$ 3.6 Å) in dimer motifs anchored at NNN Al sit well the experimentally determined value data of 3.6 Å <sup>[25]</sup> w calculated distance for a comparable NNN motif of 3.20 Å (with	hile it is considerably greater than	the DFT-
		et al. <sup>[29]</sup> . The overall discrepancies between our calculated value due to the qualitative differences between our predictions and		
36 37	20	due to the quantative differences between our predictions and	d the experimentally proposed mou	1.
38				21
				or each of the three Mooxide motifs, we have comput ed the vibratio
51 52 53 54 55 56 57				
58 59				68

### **Chemistry of Materials**

nal frequen cies for the normal <sup>[25]</sup> and 39 22 40 m odes. Compar ison of calculat ed values with previou sly reporte d Raman spectral data 23 41 ca lculatio ns<sup>[18, 29]</sup> show good overall agreem ent. Our data are reporte d in **Table S9**. 42 3.3.2. Energetics of Mo-oxides in H-ZSM-5 43 24 44 51 52 29 <sup>53</sup> 30 54 55 31 56 57 58

69

1 2		
3	1	
4	1	
5	2	
6 7	3	
, 45 2 46		In addition to predicting structures, we computed the binding energies for each structure as described
	26	in the methods section in the supporting information (SI). We have used these binding energies as a basis
48 49	27	for evaluating the relative thermodynamics of these structures to compare candidate structures within a
50 28 given motif. The binding energies of the various MoO <sub>2</sub> OH <sup>+</sup> monomers are presented as a heat map in <b>Figure</b>		
		9. For instance, MoO <sub>2</sub> OH <sup>+</sup> -8, Al 8 ( <b>Figure 1 (a)</b> ), a motif with Mo anchored atop the Al-substituted T-site,
		is predicted to be 60 kJ mol <sup>-1</sup> more stable than MoO <sub>2</sub> OH <sup>+</sup> -9, Al 8 ( <b>Figure 1 (c)</b> ) which features only one
		Mo-O <sub>F</sub> -Al coordination. The same atop-anchoring motif of Mo, MoO <sub>2</sub> OH <sup>+</sup> -8, Al 8, is 167 kJ
		Page 28 of 41
		1 460 20 01 12
		mol <sup>-1</sup> more stable than MoO <sub>2</sub> OH <sup>+</sup> -8, Al 2, a structure with the Al and Mo coordinatively separated by four
T-sites. In general, greater coordinative distance between the Al site and the site at which MoO <sub>2</sub> OH <sup>+</sup> is anchored		
results in a decrease in predicted binding energy. Therefore, for a given Al siting, it is more 8		
9	4	likely that Mo will anchor near to the Al and we expect these species to dominate observed structures.
10 11	5	While we do expect the "conventional" $MoO_2OH^+$ monomers anchored atop the Al-substituted T-site to
12		6 contribute to the Mo-oxide mixture, we note that that some structures that share only one Mo-O <sub>F</sub> -Al
13 14		<ul> <li>less stable than the atop motifs with two such coordinations,</li> <li>coordination are only 10 – 30 kJ mol</li> </ul>
15	0	complementing that these emocies are year likely to be observed in significant namedation. Consmilly
16	8	corroborating that these species are very likely to be observed in significant population. Generally,
51 52		
52 53		
54		

9 differences in binding energies of MoO<sub>2</sub>OH<sup>+</sup> monomers could be attributed to two factors: intrinsic T-site
 19 10 anchoring preferences and the coordinative separation between the Al-substituted T-site and the Mo
 20
 21 11 monomer anchoring site. Al siting is static from synthesis; therefore, only a small set of the predicted
 22 12 structures will actually be realizable at a given Al-substituted T-site in a real material. In a real sample, it
 23 is likely that some distribution of these (and similar) species would coexist with other oxide speciations 25
 24 13 (MoO<sub>2</sub><sup>2+</sup> monomers and Mo<sub>2</sub>O<sub>5</sub><sup>2+</sup> dimers), for which we discuss the energetics next.

Mo oxide T-site 1 5 9 8 7 2 6 11 12 3 1 -281 -251 -136 -244 -284 -247 -189 5 Al atom T-site -250 -291 -236 -192 6 9 -259 -271 -258 8 -143 -192 -197 -231 -291 -260 -191 -156 -147 -138 7 -253 -297 -255 11 -202 -230 -252 -298 12 -186 -270 -280 -262 -242 -271 3 -144 -299 2 -124 -247 -302

Figure 9. Binding energies (kJ mol<sup>-1</sup>) of MoO<sub>2</sub>OH<sup>+</sup> monomers anchored at single Al atom site (T-site indexing shown in **Figure 8 (a)**). These data are also presented tabularly in **Table S10**.

15

27

28 29

30 31

32

33 34

35

36 37

38

39 40

41

42 43

44 45

58

59

60 ACS Paragon Plus Environment

3 1 Table 5 DFT-calculated binding energy of isolated MoO<sub>2</sub><sup>2+</sup> monomer oxide species anchored on a double Al-atom 4 framework site.

Model characteristic	Structure	Anchoring site type	Channel type	Binding energ (kJ mol <sup>-1</sup> )
	MoO <sub>2</sub> <sup>2+</sup> -7-11 (Al 8,11)	NNN	Straight	-187
	MoO <sub>2</sub> <sup>2+</sup> -7-11 (Al 8,12)	NNNN	Straight	-153
	MoO <sub>2</sub> <sup>2+</sup> -9-9 (Al 6,9)	NNN	Sinusoidal	-226
Mo monomer on double Al-atom site	MoO <sub>2</sub> <sup>2+</sup> -9-9 (Al 6,6)	NNNN	Sinusoidal	-182
	$MoO_2^{2+}$ -12-12 (Al 3,12)	NNN	Sinusoidal	-220
	MoO <sub>2</sub> <sup>2+</sup> -12-12 (Al 3,3)	NNNN	Sinusoidal	-188
	MoO <sub>2</sub> <sup>2+</sup> -10-10 (Al 1,10)	NNN	Sinusoidal	-215
	MoO <sub>2</sub> <sup>2+</sup> -10-10 (Al 1,1)	NNNN	Sinusoidal	-185

  **Table 5** provides the DFT-calculated binding energies of MoO<sub>2</sub><sup>2+</sup> motifs anchored on double Al

2+ species to anchor at Al-Al
5 framework sites. As shown in **Table 5**, there is a weak preference for MoO<sub>2</sub>

6 pairs in the NNN (Al-Si-O-Si-Al) arrangement. It should be noted that intrinsic Al siting in the H-ZSM-5

27 28

29

34

56 57 58

59

- 7 is responsible for part of the observed binding energy differences: more stable Al siting generally leads
- 30 8 to weaker binding of an external species. The NNNN (Al-(Si-O)<sub>2</sub>-Al) arrangement serves as a less
- 31 9 favorable anchoring site for  $MoO_2^{2+}$ ; the two  $Al^{3+}$  are sited farther away from one another, and bonding 32
- of Mo to two O<sub>F</sub> induces a greater distortion in the framework than in NNN motifs.
- 35 11 Table 6. DFT-calculated binding energy of isolated Mo dimer oxide species anchored on a double Al-atom
- 36 12 framework site.

37		
38		Model characteristic Structure Anchoring site type Channel type Binding energy (kJ mol <sup>-1</sup> )
40		<sup>2+</sup> -8,12 (Al 8,11) NNN Straight -491 Mo <sub>2</sub> O <sub>5</sub>
41		MO2O5
42		Mo <sub>2</sub> O <sub>5</sub> <sup>2+</sup> -8,12 (Al 8,12) NNNN Straight -552
43		Mo <sub>2</sub> O <sub>5</sub> <sup>2+</sup> -6,6 (Al 6,9) NNN Sinusoidal -487
44		
45	$Mo_2O_5^{2+}$ -6,6 (Al 6,6) NNNN Sinusoidal -546	
46		inusoidal -549
47	double Al-atom site	
48	$Mo_2O_5^{2+}$ -3,3 (Al 3,3) NNNN Sinusoidal -606	
49	Mo <sub>2</sub> O <sub>5</sub> <sup>2+</sup> -1,1 (Al 1,10) NNN Sinusoidal -496	
50	<sup>2+</sup> -1,1 (Al 1,1) NNNN Sinusoidal -562 Mo <sub>2</sub> O <sub>5</sub>	
	Mo <sub>2</sub> O <sub>5</sub> <sup>2+</sup> -3,7 (Al 3,7) NNNN Straight	-568
51		
52		
53		
54		
55		

Mo <sub>2</sub> O <sub>5</sub> <sup>2+</sup> -3,7 (Al 3,8)	NNNNN	Straight
Mo <sub>2</sub> O <sub>5</sub> <sup>2+</sup> -2,8 (Al 2,8)	NNNNN	Straight

Page 30 of 41

Mo<sub>2</sub>O<sub>5</sub><sup>2+</sup>-3,11 (Al 2,7)

NNNNNN

Straight

-496

-486 -446

1

2 **Table 6** provides the DFT-calculated binding energies of the Mo<sub>2</sub>O<sub>5</sub><sup>2+</sup> dimers anchored on different

8

double Al framewor k sites. As shown in **Table 6**, Mo<sub>2</sub>O<sub>5</sub><sup>2+</sup> interacts more favorably with NNNN (Al-(Si-

9 10 [29]. We do 4 O)<sub>2</sub>-Al) arrangeme nts of Al substitutio ns, in agreement

51 52 53

58 59 60

57

ACS Paragon Plus Environment

•	1	1		
•	ı	4	-	

5 not expect these energetics to affect speciation because Al siting distributions arise during zeolite 12

6 synthesis, anchoring of the monomer precursor species (MoO<sub>2</sub>OH<sup>+</sup>) happens independently, and

13 14 15

formation of the Mo<sub>2</sub>O<sub>5</sub><sup>2+</sup> dimer can be regarded as irreversible and possible if two monomers exist in

16 17 7

appropriate proximity to one another. Thus, the main utility of the energies here is in demonstrating that

18

these dimers may at least be thermodynamically competitive with the MoO<sub>2</sub>OH<sup>+</sup> monomer species.

20 10 21

19

We note that the energies computed for all motifs and the comparisons between them often rely on

22 11

zeolites with different Al sitings, limiting the utility of directly comparing some reported energies.

23 24

Moreover, the irreversibility of formation/anchoring/interconversion of MoO<sub>x</sub> species as shown in **Figure** 

25 26

13 2 (due to disproportionation of H<sub>2</sub>O) is expected to result in kinetic trapping, and therefore global

27 14 28

thermodynamic minima are not expected to be explored. Nonetheless, comparing relative energetics of

29

species of like motif with similar Al sitings can be useful in building insights into which species are 15 most

probable to observe, and the database of structures we have built through this study forms a strong basis

30

16 31

32

for comparison to experimentally measured spectral data. To corroborate our computational DFT 33 17 investigations, experimental TPO measurements, and operando XAS spectroscopy, we employ theory-

34 18 35

guided X-ray absorption spectroscopy (QuantEXAFS) to evaluate the speciation of isolated Mo-oxides on

36

37 20

H-ZSM-5 prepared via different synthesis techniques (PM vs. IWI) and Mo loadings (1, 3 wt.%) by 38

39 21 mapping the experimental XAS spectra to the model spectra from DFT-predicted structures.

40

41

22 3.4. QuantEXAFS/DFT: Active Site Identification

51 52 53

54 55 56

57 58

59 60

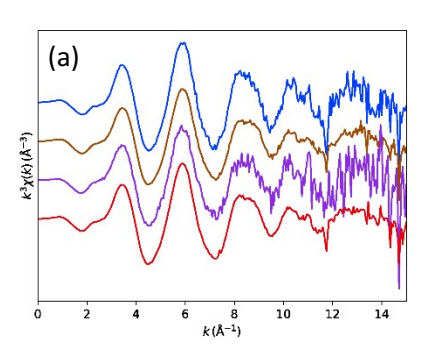
1 2 3 4 5 6		
7 42 43		[40] was employed to compare 23 Theory-guided X-ray absorption spectroscopy analysis (QuantEXAFS)
44		24 our DFT-predicted Mooxide structures to experimentally measured EXAFS spectra to aid in our analysis
45 46 2 47	.5	of Mo-oxide speciation in our TPO experiments. QuantEXAFS combines the systematic DFT calculations
48 2 49	6	of potential stable $\text{MoO}_{x}$ structures with automated analysis of EXAFS data with the aim of determining
50 2	7	the location and motif of the Mo-oxides in H-ZSM-5. In this study using QuantEXAFS, we have analyzed
	28 1	four samples differing in synthesis technique (IWI and PM), and Mo loading (1 wt.% and 3 wt.%) with 29 H-
	ZS	M-5 of consistent acidity at $Si/Al = 15$ .
Page	31	of 41
1 2		
3 4	1	While our DFT calculations have demonstrated that each of the three qualitatively distinct Mo-oxide
5 6	2	motifs is thermodynamically reasonable, our commentary thus far on which species we expect to observe
7 8	3	has been based on interpretation of TPO results, which provides indirect evidence of Mo-oxide local
9	4	structures. By using our DFT-predicted structures as a database for comparison to our experimentally
10 51 52 53 54 55 56 57	5	measured EXAFS spectra, we demonstrate that the measured spectra are consistent with the spectra that
58 59		76

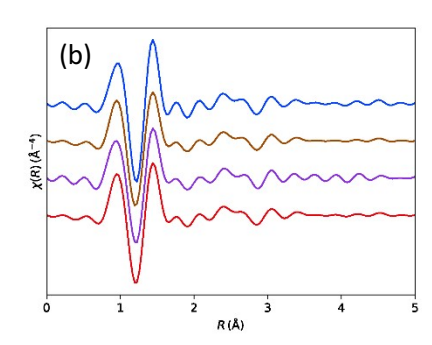
29 10

41 17 

could arise from the distinct motifs represented among our model structures. Figure 10 shows the experimentally measured Mo K-edge EXAFS data, which we additionally note exhibit distinct characteristics between different Mo loadings and/or preparation methods, suggesting that the spectral

differences observed may be attributed to both metal loading and catalyst preparation method.





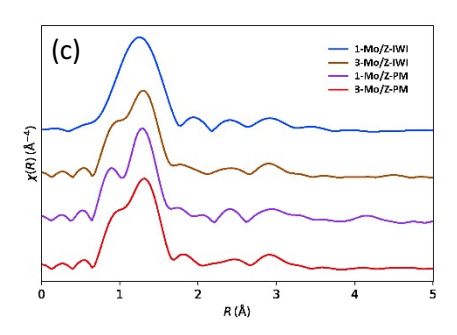


Figure 10. Experimental EXAFS data, (a) k-space (2.0-14.0 Å<sup>-1</sup>), R-space (b) imaginary part, and (c) magnitude (0.5-5.0 Å).

For 1-Mo/Z-IWI (15), we find that the structures that best fit are all MoO<sub>2</sub>OH<sup>+</sup> motifs, suggesting a preponderance of isolated oxide monomers in samples prepared in this way. This is consistent with what we would expect for a low metal loading prepared via IWI, where we reason that the impregnation method lends to better dispersion of metal oxide species over PM, where the mechanism for impregnation is diffusion of external material into the zeolite pore at elevated temperatures. Notably, we also expect to see MoO<sub>2</sub><sup>2+</sup> monomeric species in samples prepared in this way because the higher acidity of zeolite and low loading is expected to lead to availability of the requisite double Al sites for this motif. However, from the set of structures from DFT that we used to fit the EXAFS spectra, no MoO<sub>2</sub><sup>2+</sup> species were identified among the best fits. In 3-Mo/Z-IWI (15), MoO<sub>2</sub><sup>2+</sup> monomers were among the best fits along

1	
2	
3	
4	
5	
6	
7	
49	
50	22

with the MoO<sub>2</sub>OH<sup>+</sup> monomers that also fit 1-Mo/Z-IWI (15). We additionally identify dimeric Mo<sub>2</sub>O<sub>5</sub><sup>2+</sup>

among the best fits for 3-Mo/Z-IWI (15). This is consistent with our expectations for a sample with increased Mo loading, where it is more probable for two anchored MoO<sub>2</sub>OH<sup>+</sup> monomers to exist anchored in proximity to one another such that they may condense to form the Mo dimeric species. We show an

- 4 5, Al 8, which is not among the most stable structures for Al at T-site 8. Because all DFT-predicted
- 5 structures are ground state (T = 0 K) calculations, it is likely that thermal motion and variation in local
- 6 structure may be contributing to the experimental observations and that off-minimum features not captured

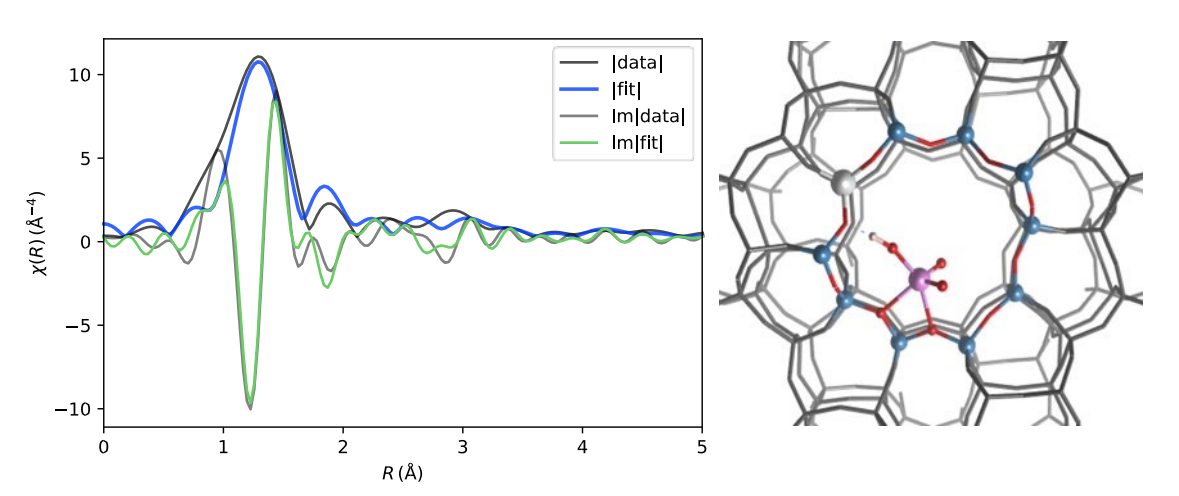


Figure 11. Experimentally measured EXAFS spectra, predicted spectra from the DFT structure, and the DFT-predicted structure ( $MoO_2OH^{^+}$ -5, Al 8), for sample 1-Mo/Z-IWI (15) (k-range 3.0–11.5 Å $^{^-1}$  and R-range 1.0–5.0 Å).

- 7 in the DFT structures contribute to spectra observed. It is reasonable also that at elevated temperatures
- 8 structures that are not the most probable will be dynamically explored by the system, although the stability
- of the identified structure,  $MoO_2OH^+$ -5, Al 8, is ~100 kJ mol<sup>-1</sup> less stable than the most stable comparable

1 2			
3	1		
4 5 6 7			
40		10 monomer with Al at T-site 8, and it is unlikely that this specific structure is to be observe Nonetheless,	d.
41 42		the slight differences among DFT-predicted structures for each motif allow for consideration of the way	/S
43		these motifs may manifest in H-ZSM-5 and for identification of spectral signatures that may indicatheir	te
44 45 1 46	L <b>3</b>	presences.	
47 1 48	<u>4</u>	Considering the samples prepared via physical mixing, 1-Mo/Z-PM (15) shows good fits of EXAF	S
49 1	15	$spectra\ to\ both\ isolated\ MoO_2OH^+\ monomer\ motifs\ as\ well\ as\ Mo_2O_5{}^{2+}\ dimer\ motifs,\ even\ at\ low\ metal\ 5-colored$	0
	<b>16</b> ]	oadings. We attribute this to the likelihood of poor dispersion and spatial clustering of anchored oxides	17
	due	to the temperature and mechanism of metal oxide impregnation in PM-prepared samples. We note 18 th	at
	the	two dimeric Mo <sub>2</sub> O <sub>5</sub> <sup>2+</sup> species identified as best fits are one each of NNN- and NNNN-type siting	
Pag	19 e 33	of Al, supporting that these species may form on either Al siting arrangement. Notably we do not identi of 41	fy
1 2			
3 4	1	any best-fit candidates among dimer motifs with coordinative separation of Al sites greater than NNNN	1.
5 6	2	The same observations for 1-Mo/Z-PM (15) apply for 3-Mo/Z-PM (15), where monomeric MoO <sub>2</sub> OH <sup>+</sup> a	nd
7 8	3	dimeric Mo <sub>2</sub> O <sub>5</sub> <sup>2+</sup> provide the best fits. For monomeric species, we identify a comparable but not identic	al
9	4	set as in the case of 1-Mo/Z-PM (15). For dimeric species, we again identify both NNN- and NNNN-type	;
51 52 53 54 55 56 57 58			
59			80

# Chemistry of Materials

10 11	5	Al sitings among the best fits. The absence of MoO <sub>2</sub> <sup>2+</sup> monomeric species among best fits is both notable
12		6 and consistent with our expectations. We attribute this to the likely spatial clustering of the impregnated
13 14		2+ species requires an 7 Mo-oxide in the zeolite pore, regardless of metal loading. Formation of the MoO <sub>2</sub>
15		+ species to exist in proximity to a vacant BAS such that disproportionation of a water 16 8 anchored MoO <sub>2</sub> OH
17 18	9	molecule may occur. Because of the likely spatial clustering of Mo-oxides in PM preparations, these sites
19 20	10	are less likely to arise, even at low metal loadings in relatively acidic zeolites. A complete accounting of
21	11	our stable structures that give reasonable EXAFS fits for IWI- and PM-prepared samples are reported in
22 23	12	the Supporting Information in Figures S9-12 and Table S11. The respective QuantEXAFS fitting
24 25	13	parameters including the $\sigma\sigma^2$ , bond distances, and $\Delta E_0$ are presented in <b>Table S12</b> . The identified stable
26 27	14	structures that give reasonable EXAFS fits (those that have an R-factor value of <0.2 and have realistic
28	15	EXAFS fit parameters) and are consistent with our other experimental results are summarized in <b>Figure</b>
29 30	16	12 and presented as a function of synthesis technique and metal loading.
31	17	When performing preliminary catalytic activity measurements contrasting the activity of the catalysts
51 52 53 54 55 56 57 58		
59 60		ACS Paragon Plus Environment

1 2		
3	1	
4	1	
5		
6		
7		
32		
33	18	prepared by IWI and PM with 4 wt.% Mo loading in MDA we found that that possible subtle differences
34 35	19	in structures of the Mo-oxide species due to different synthesis methods did not lead to significant
36 37	20	differences in the catalytic performance (Figure S13). This is not entirely surprising as catalyst activation
38 39	21	for MDA is achieved by reducing the Mo-oxide species under high temperature reducing conditions and
40	22	the effect of the Mo-oxide structure on the reduced Mo sites is not yet known. Furthermore, this result
41 42	23	aligns with previous work in which researchers employing these different synthesis techniques still
43 44	24	achieve very similar benzene yields when employing similar Mo loadings. However, we also note that the
45 46	25	reactor employed for our measurements only provides global average kinetic data and may not allow for
47	26	a distinction in the intrinsic kinetics resulting from the different Mo-oxide speciation. Rigorous evaluation
48 49	27	of the microkinetic details and the intrinsic kinetics of the catalysts prepared by the different synthesis
50	28	techniques would require performing transient kinetic experiments, for instance in a temporal analysis of 29
		products (TAP) reactor, which are not within the scope of the work we are presenting here.
	30	31

Page 34 of 41

# 4. Conclusions

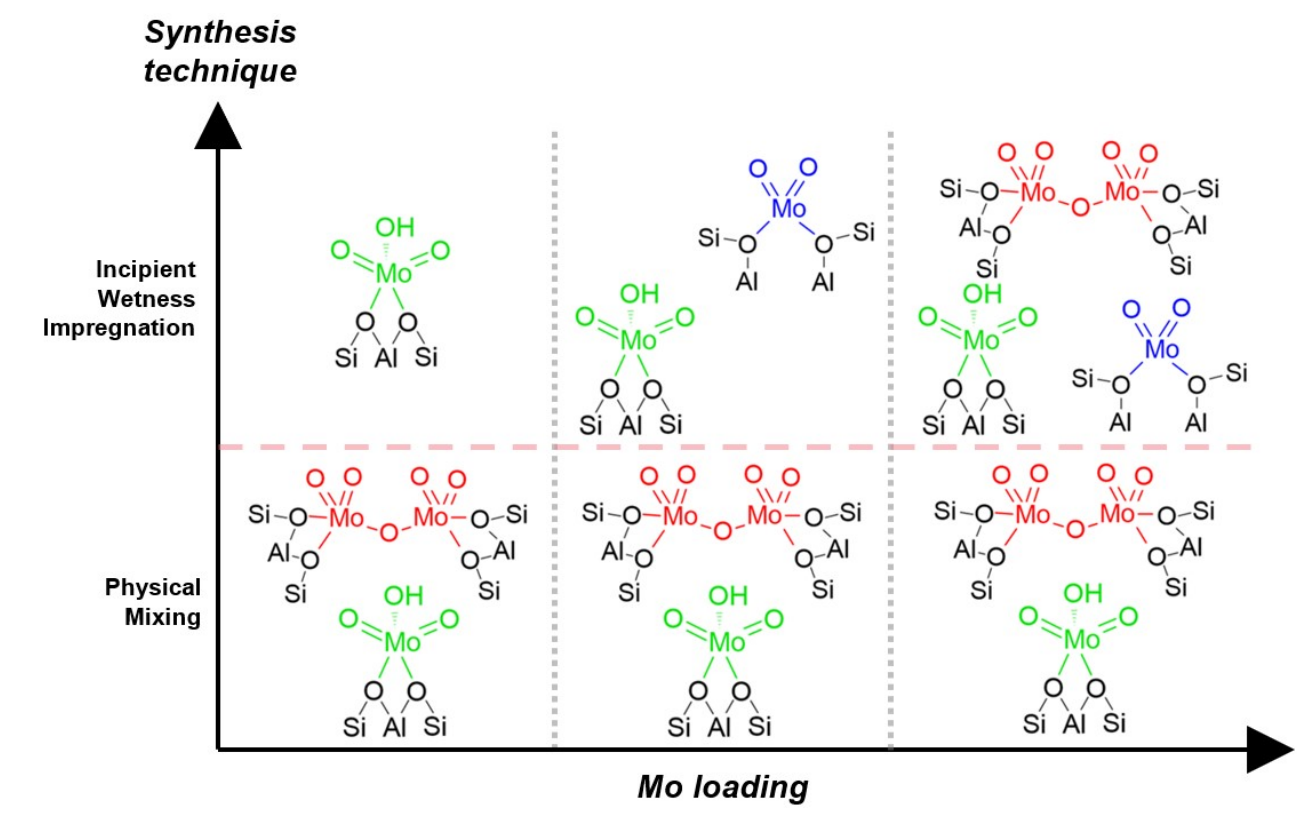


> Figure 12. Summary of most probable Mo-oxide species in Mo/H-ZSM-5 as affected by synthesis technique and Mo loading.

In the preceding work, we have presented fundamental and synergistic experimental and computational investigations of H-ZSM-5 impregnated with Mo-oxides as a platform system for building 7 broader understanding of the effects of metal loading and impregnation method on the resultant metal oxide speciation in acidic zeolites. We have selected this system for its relevance as a prominent catalyst

10 metal oxides impregnated in zeolites are of interest for a variety of applications in catalysis. We have used

with yet-unsettled fundamental questions about its nature in the literature around MDA, but we note that

2	1	
4 5 6	1	
7 44	11	a combination of TPO experiments, XANES and EXAFS experiments, DFT calculations, and
45 46 1 47	.2	QuantEXAFS analysis to investigate the speciation of Mo-oxides in H-ZSM-5, establishing that the metal
48 1 49	.3	oxide catalyst precursors are likely to exist in multiple qualitatively distinct motifs, and that the
50 1	.4	distribution of motifs observed may be controlled to a limited extent through amount of metal oxide added
	15	to the zeolite as well as through the method in which the metal oxide is impregnated into the zeolite. In
	16	our analysis, we have considered the three most proposed motifs for Mo-oxides in H-ZSM-5. Because
Page	17 e 35	these motifs, $MoO_2OH^+$ , $MoO_2^{2+}$ , and $Mo_2O_5^{2+}$ , each are understood to anchor differently within the H-of 41
1 2		
3	1	ZSM-5 channels at Brønsted acidic sites, quantified evolution of H <sub>2</sub> O during TPO provides evidence for
5	2	differences in the distributions of these anchored species in terms of the H/Mo ratio observed. Our TPO
7	3	experiments demonstrate that IWI preparations result in more water evolution per metal anchored relative
9	4	to PM preparations, indicating different distributions of Mo-oxide species between these preparations.
10 11	5	TPO further provides evidence that anchoring occurs at different temperatures via monitoring
12 13	6	temperature-dependent evolution of $H_2O$ , with IWI-prepared metal oxides anchoring at $200-500\ ^{\circ}C$ and
14	7	PM-prepared oxides anchoring at $350-700^{\circ}$ C. These results are corroborated and further supported by
15 16	8	complementary operando XANES experiments showing temperature-dependent evolution of the Mo K-
51 52 53 54 55 56 57 58		
59		82

## Chemistry of Materials

17 18	9	edge consistent with changes in local Mo coordination consistent with our TPO results. Our measured
19 20	10	EXAFS spectra also serve as inputs complementary to our suite of DFT-predicted structures in our
21	11	QuantEXAFS analysis. To establish a database of structures for QuantEXAFS analysis and to understand
22 23	12	the ways in which these various Mo-oxide motifs may manifest in H-ZSM-5, we performed DFT
24 25	13	calculations on 42 $MoO_2OH^+$ monomeric oxides, eight $MoO_2^{2+}$ monomeric oxides, and 12 $Mo_2O_5^{2+}$
26 27	14	dimeric oxides to form a database of 62 unique candidate structures. Our DFT calculations characterize
	15	these oxide structures and demonstrate that Mo-oxides may viably anchor in a variety of ways in H-ZSM-
29 31 32		5. Notably, our DFT calculations demonstrate that, while not energetically favored, it is feasible for Mo30 oxides to anchor in the vicinity of BAS without direct coordination to the BAS and that dimeric Mo-oxides
33	18	may form from condensation of monomers anchored near Al-substituted T-sites of greater separation than
34 35	19	the Al siting restrictions necessary for formation of MoO <sub>2</sub> <sup>2+</sup> monomeric species. We combine our EXAFS
36 37	20	spectra with our DFT-predicted structures in QuantEXAFS analysis to identify from among our candidate
38 39	21	structures which provide best-fit agreement with measured spectra. Through this analysis we find that
40	22	both metal loading $(1-3 \text{ wt.}\% \text{ Mo})$ and impregnation method (IWI vs. PM) lead to different EXAFS
41 42	23	spectra, which are best-fit by qualitatively different Mo-oxide motifs. Samples prepared with IWI showed
43 44	24	spectra consistent with a greater prevalence of monomeric Mo-oxides, with increased metal loading
45 46	25	resulting in spectra suggesting formation of more dimeric species. This is consistent with the
	26	understanding of IWI leading to better dispersion of smaller Mo-oxides within H-ZSM-5 prior to
48 49	27	anchoring at higher temperatures. Complementarily, PM-prepared samples indicated a presence of dimeric
50	28	oxide species even at the lowest loading of 1 wt.%, consistent with the understanding of the anchoring
2	29	mechanism of larger oxide particles breaking up and diffusing as smaller agglomerates only at
51		
52 53		
54		
55		
56 57		
<i>J</i> /		

temperatures already capable of facilitating anchoring of these oxides at BAS of H-ZSM-5, resulting in 31 overall lower metal oxide dispersion.

7

9

10 11

12 13

15

16

17 18

20

27

28 15 29

30 16

Page 36 of 41

Overall, we have brought complementary experimental and theoretical techniques together to build an improved understanding of Mo-oxides in H-ZSM-5, a catalytically relevant system for MDA catalysis.

- 3 Our work suggests and supports the existence of a distribution of Mo-oxides in H-ZSM-5 comprised of a 8
  - 4 combination of various qualitatively distinct motifs reported in previous literature. We additionally
  - 5 provide evidence that the catalyst precursor synthesis approach leads to different abundances of the
- 6 various oxide species, an observation that can reconcile some of the long-standing lack of consensus
- 14 7 surrounding these systems. We rationalize our observations through consideration of the impregnation
  - 8 methods and the likely processes underlying the anchoring of these catalyst precursors. This work thus
  - 9 provides for the first time a rational understanding and basis for engineering speciation of oxides through
- 19 10 choice of preparation method and metal loading. While it is yet unsettled what implications these various
- 21 11 anchored oxide motifs may have on the structure, stoichiometry, and performance of the activated
- 22 12 (carburized) Mo sites, understanding the precursors is a necessary first step toward rational design of next23
- 24 13 generation MDA catalysts. Additionally, we envision that the conclusions drawn and the techniques 25
- 26 14 employed may naturally extend to other comparable metal-oxide/zeolite composite materials.

# 5. Acknowledgements

This work was supported by the United States of America National Science Foundation Award

51

56 57 58

_		
3	1	
4		
5 6 7 31	2	
	17	#2005324. This research used resources of the Stanford Synchrotron Radiation Lightsource. Use of the
33 35 36	18 19	Stanford Synchrotron Radiation Lightsource, SLAC National Accelerator Laboratory, is supported by the 34 U.S. Department of Energy, Office of Science, Office of Basic Energy Sciences under Contract No. DE-
37		20 AC02-76SF00515. Co-ACCESS is supported by the U.S. Department of Energy, Office of Basic Energy
38 39		Sciences, Chemical Sciences, Geosciences and Biosciences Division. R.R. thanks Prof. Kulkarni for the 21
40 41		useful discussions. J.D.H. and F.M. additionally graciously acknowledge support of computational
42 43	23	components of work performed at Texas Tech from the Texas Tech University High Performance
44	24	Computing Center.
45		
46 47	25	6. Supporting Information
48 49	26	The Supporting Information is available free of charge at [URL]. Experimental and computational
50	27	methods, nomenclature, TPO results, TPO-XAS results, reactivity data, DFT-predicted structures and 28
	pro	perties, and QuantEXAFS data (.docx). Electronic supporting information (*.zip) contains VASP 29 structure
	file	es for 62 DFT-predicted structures and Excel sheet containing descriptive names of each
Pag	30 ge 37	structure file. of 41
1		
51 52 53 54 55 56 57		
58		

### 3 1 References

4 Reference

- 5 2 [1] E.T. Vogt, B.M. Weckhuysen, Fluid catalytic cracking: recent developments on the grand old lady of zeolite 6 3 catalysis, Chemical Society Reviews, 44 (2015) 7342-7370.
- 7 4 [2] V. Blay, B. Louis, R.n. Miravalles, T. Yokoi, K.A. Peccatiello, M. Clough, B. Yilmaz, Engineering zeolites
- for 8 5 catalytic cracking to light olefins, ACS Catalysis, 7 (2017) 6542-6566.
- 9 6 [3] T. Ennaert, J. Van Aelst, J. Dijkmans, R. De Clercq, W. Schutyser, M. Dusselier, D. Verboekend, B.F. Sels, 10
- 7 Potential and challenges of zeolite chemistry in the catalytic conversion of biomass, Chemical Society
- Reviews, 12 8 45 (2016) 584-611.
- 9 [4] F. Su, Y. Guo, Advancements in solid acid catalysts for biodiesel production, Green Chemistry, 16 (2014)
- 14 10 2934-2957.
- 15 11 [5] N. Kosinov, E.J.M. Hensen, Reactivity, Selectivity, and Stability of Zeolite-Based Catalysts for Methane 16 12 Dehydroaromatization, Advanced Materials, Wiley-VCH Verlag, (2020) 2002565.
- 17 13 [6] U. Menon, M. Rahman, S.J. Khatib, A Critical Literature Review of the Advances in Methane
- Dehydroaromatization over Multifunctional Metal-Promoted Zeolite Catalysts, Applied Catalysis A: General, 19
   (2020) 117870.
- 16 [7] A.I. Olivos-Suarez, À. Szécsényi, E.J. Hensen, J. Ruiz-Martinez, E.A. Pidko, J. Gascon, Strategies for the direct 22 17 catalytic valorization of methane using heterogeneous catalysis: challenges and opportunities, Acs Catalysis, 6 23 18 (2016) 2965-2981.
- 24 19 [8] P. Schwach, X. Pan, X. Bao, Direct conversion of methane to value-added chemicals over heterogeneous 25 20 catalysts: challenges and prospects, Chemical reviews, 117 (2017) 8497-8520.
- 26 21 [9] I. Yarulina, A.D. Chowdhury, F. Meirer, B.M. Weckhuysen, J. Gascon, Recent trends and fundamental insights
- 27 22 in the methanol-to-hydrocarbons process, Nature Catalysis, 1 (2018) 398-411.
- 29 23 [10] S. Ilias, A. Bhan, Mechanism of the catalytic conversion of methanol to hydrocarbons, Acs Catalysis, 3 (2013)
- 30 24 18-31.

28

- 25 [11] V. Van Speybroeck, K. De Wispelaere, J. Van der Mynsbrugge, M. Vandichel, K. Hemelsoet, M. Waroquier, 32 26 First principle chemical kinetics in zeolites: the methanol-to-olefin process as a case study, Chemical Society 33 27 Reviews, 43 (2014) 7326-7357.
- 34 28 [12] T. Andana, K.G. Rappé, F. Gao, J. Szanyi, X. Pereira-Hernandez, Y. Wang, Recent advances in hybrid metal 35 29 oxide—zeolite catalysts for low-temperature selective catalytic reduction of NOx by ammonia, Applied Catalysis 36 30 B: Environmental, 291 (2021) 120054.
- 37 31 [13] F. Gramigni, U. Iacobone, N.D. Nasello, T. Selleri, N. Usberti, I. Nova, Review of hydrocarbon poisoning and 38 deactivation effects on Cu-Zeolite, fe-zeolite, and vanadium-based selective catalytic reduction catalysts for nox 40
- removal from lean exhausts, Industrial & Engineering Chemistry Research, 60 (2021) 6403-6420.

51 52

53 54

55

56 57

58

59

1 2 3 1 4 2 5 6 7 41 34 [14] A.M. Beale, F. Gao, I. Lezcano-Gonzalez, C.H. Peden, J. Szanyi, Recent advances in automotive catalysis for 42 35 36

NO x emission control by small-pore microporous materials, Chemical Society Reviews, 44 (2015) 7371-7405. 43 [15] R. Zhang, N. Liu, Z. Lei, B. Chen, Selective transformation of various nitrogen-containing exhaust gases 44 37 toward N2 over zeolite catalysts, Chemical reviews, 116 (2016) 3658-3721.

45 38 [16] P. Granger, V.I. Parvulescu, Catalytic NO x abatement systems for mobile sources: from three-way to lean 46 39 burn after-treatment technologies, Chemical Reviews, 111 (2011) 3155-3207. 47

48 40 [17] N.K. Razdan, A. Bhan, Carbidic Mo is the sole kinetically-relevant active site for catalytic methane 49 41 dehydroaromatization on Mo/H-ZSM-5, Journal of Catalysis, 389 (2020) 667-676.

50 42 [18] J. Gao, Y. Zheng, J.-M. Jehng, Y. Tang, I.E. Wachs, S.G. Podkolzin, Identification of molybdenum oxide 43 nanostructures on zeolites for natural gas conversion, Science, 348 (2015) 686-690.

44 [19] M. Rahman, A. Infantes-Molina, A.S. Hoffman, S.R. Bare, K.L. Emerson, S.J. Khatib, Effect of Si/Al ratio of 45 ZSM-5 support on structure and activity of Mo species in methane dehydroaromatization, Fuel, 278 (2020) 46 118290.

Page 38 of 41

[20] K. Sun, D.M. Ginosar, T. He, Y. Zhang, M. Fan, R. Chen, Progress in Nonoxidative Dehydroaromatization of Methane in the Last 6 Years, Industrial & Engineering Chemistry Research, 57 (2018) 1768-1789.

- [21] N. Kosinov, F.J. Coumans, E.A. Uslamin, A.S. Wijpkema, B. Mezari, E.J. Hensen, Methane 3
- dehydroaromatization by Mo/HZSM-5: mono-or bifunctional catalysis?, ACS Catalysis, 7 (2017) 520-529.
- 5 [22] R.W. Borry, Y.H. Kim, A. Huffsmith, J.A. Reimer, E. Iglesia, Structure and density of Mo and acid sites in Mo9 6 exchanged H-ZSM5 catalysts for nonoxidative methane conversion, Journal of Physical Chemistry B, American 10 Chemical Society, 1999, pp. 5787-5796.
- 11 8 [23] I. Vollmer, G. Li, I. Yarulina, N. Kosinov, E.J. Hensen, K. Houben, D. Mance, M. Baldus, J. Gascon, F. Kapteijn, 12 Relevance of the Mo-precursor state in H-ZSM-5 for methane dehydroaromatization, Catalysis Science and
- Technology, Royal Society of Chemistry, 2018, pp. 916-922. 13 10

57 58

59 60

42

- 15 11 [24] Y.H. Kim, R.W. Borry, E. Iglesia, Genesis of methane activation sites in Mo-exchanged H-ZSM-5 catalysts, 16 12 Microporous and Mesoporous Materials, 2000, pp. 495-509.
- 17 13 [25] W. Li, G.D. Meitzner, R.W. Borry, E. Iglesia, Raman and X-ray absorption studies of Mo species in Mo/H18 14 ZSM5 catalysts for non-oxidative CH4 reactions, Journal of Catalysis, Academic Press Inc., 2000, pp. 373-383.
- 19 15 [26] Y. Zheng, Y. Tang, J.R. Gallagher, J. Gao, J.T. Miller, I.E. Wachs, S.G. Podkolzin, Molybdenum Oxide,
- 20 16 Oxycarbide, and Carbide: Controlling the Dynamic Composition, Size, and Catalytic Activity of Zeolite-Supported 21
- 17 Nanostructures, Journal of Physical Chemistry C, American Chemical Society, 2019, pp. 22281-22292.
- 22 18 [27] S. Ma, X. Guo, L. Zhao, S. Scott, X. Bao, Recent progress in methane dehydroaromatization: From laboratory 23
- 24 19 curiosities to promising technology, Journal of Energy Chemistry, Elsevier B.V., 2013, pp. 1-20.
- 25 20 [28] M. Agote-Arán, A.B. Kroner, H.U. Islam, W.A. Sławiński, D.S. Wragg, I. Lezcano-González, A.M. Beale, 26 21

  Determination of Molybdenum Species Evolution during Non-Oxidative Dehydroaromatization of Methane and 27
  - 22 its Implications for Catalytic Performance, ChemCatChem, Wiley Blackwell, 2019, pp. 473-480.
- 28 23 [29] D. Zhou, Y. Zhang, H. Zhu, D. Ma, X. Bao, The structure, stability, and reactivity of mo-oxo species in H-ZSM5 29
- zeolites: Density functional theory study, Journal of Physical Chemistry C, 2007, pp. 2081-2091.
- 30 25 [30] I. Lezcano-González, R. Oord, M. Rovezzi, P. Glatzel, S.W. Botchway, B.M. Weckhuysen, A.M. Beale, 31 26 Molybdenum Speciation and its Impact on Catalytic Activity during Methane Dehydroaromatization in Zeolite
- 32 27 ZSM-5 as Revealed by Operando X-Ray Methods, Angewandte Chemie, 2016, pp. 5301-5305.
- 34 28 [31] J.P. Tessonnier, B. Louis, S. Walspurger, J. Sommer, M.J. Ledoux, C. Pham-Huu, Quantitative measurement 35
- of the Brönsted acid sites in solid acids: Toward a single-site design of Mo-modified ZSM-5 zeolite, Journal of 36
- 30 Physical Chemistry B, 2006, pp. 10390-10395.
- 37 31 [32] J.-P. Tessonnier, B. Louis, S. Rigolet, M.J. Ledoux, C. Pham-Huu, Methane dehydro-aromatization on 38 32 Mo/ZSM-5: About the hidden role of Brønsted acid sites, Applied Catalysis A: General, 336 (2008) 79-88.
- 39 33 [33] A. Kumar, K. Song, L. Liu, Y. Han, A. Bhan, Absorptive Hydrogen Scavenging for Enhanced Aromatics Yield 40 34 During Non-oxidative Methane Dehydroaromatization on Mo/H-ZSM-5 Catalysts, Angewandte Chemie
- 41 35 International Edition, 57 (2018) 15577-15582.
- 43 36 [34] N.K. Razdan, A. Kumar, B.L. Foley, A. Bhan, Influence of ethylene and acetylene on the rate and reversibility 44
- of methane dehydroaromatization on Mo/H-ZSM-5 catalysts, Journal of Catalysis, 381 (2020) 261-270.
- 45 38 [35] H.S. Lacheen, E. Iglesia, Stability, structure, and oxidation state of Mo/H-ZSM-5 catalysts during reactions of 46
- 39 CH4 and CH4–CO2 mixtures, Journal of Catalysis, 230 (2005) 173-185.
- 47 40 [36] H.S. Lacheen, E. Iglesia, Isothermal activation of Mo 2 O 5 2+–ZSM-5 precursors during methane reactions:
- 48 41 effects of reaction products on structural evolution and catalytic properties, Physical Chemistry Chemical 49 42 Physics, 7 (2005) 538-547.

#### **Chemistry of Materials**

1	
2	
3	1
4	
5	2
6	
7	

50 43 [37] W. Ding, S. Li, G. D Meitzner, E. Iglesia, Methane conversion to aromatics on Mo/H-ZSM5: structure of 44 molybdenum species in working catalysts, The Journal of Physical Chemistry B, 105 (2001) 506-513.

[38] I.K. van Ravenhorst, A.S. Hoffman, C. Vogt, A. Boubnov, N. Patra, R. Oord, C. Akatay, F. Meirer, S.R. Bare,
 B.M. Weckhuysen, On the Cobalt Carbide Formation in a Co/TiO2 Fischer—Tropsch Synthesis Catalyst as Studied
 by High-Pressure, Long-Term Operando X-ray Absorption and Diffraction, ACS Catalysis, 11 (2021) 2956-2967.

1 2	
3 1 4	[39] C. Vogt, F. Meirer, M. Monai, E. Groeneveld, D. Ferri, R.A. van Santen, M. Nachtegaal, R.R. Unocic, A.I.
5	2 Frenkel, B.M. Weckhuysen, Dynamic restructuring of supported metal nanoparticles and its
implica	ations for 6 3 structure insensitive catalysis, Nature Communications, 12 (2021) 7096.
7 Theory Dispers	4 [40] Y. Chen, R. Rana, T. Sours, F.D. Vila, S. Cao, T. Blum, J. Hong, A.S. Hoffman, CY. Fang, Z. Huang, A 5 Guided X-ray Absorption Spectroscopy Approach for Identifying Active Sites in Atomically sed Transition9 6 Metal Catalysts, Journal of the American Chemical Society, 143 (2021) 20144-20156.
10	7 [41] M. Rahman, A. Sridhar, S.J. Khatib, Impact of the presence of Mo carbide species prepared ex situ in
11	8 Mo/HZSM-5 on the catalytic properties in methane aromatization, Applied Catalysis A: General, 558
(2018) 12 9	67- 80.
13 10	[42] A.S. Hoffman, J.A. Singh, S.F. Bent, S.R. Bare, In situ observation of phase changes of a silica-
15 11 12 13 14	cobalt catalyst for the Fischer–Tropsch process by the development of a synchrotron-compatible in 16 situ/operando powder X-ray diffraction cell, Journal of Synchrotron Radiation, 25 (2018) 1673-1682. 17 [43] A.S. Hoffman, catXAS, https://github.com/ahoffm02/catXAS, 2021, pp. In-situ catalysis XAS data 18 manipulation and analysis package for data collected at SSRL using the CXAS software.
19 15	[44] B. Ravel, M. Newville, ATHENA, ARTEMIS, HEPHAESTUS: data analysis for X-ray absorption spectroscopy 20
16	using IFEFFIT, Journal of Synchrotron Radiation, 12 (2005) 537-541.
21 17	[45] G. Kresse, D. Joubert, From ultrasoft pseudopotentials to the projector augmented-wave method, Physical
22 18 23	review b, 59 (1999) 1758.
24 19	[46] P.E. Blöchl, Projector augmented-wave method, Physical review B, 50 (1994) 17953.
25 20	[47] J.P. Perdew, K. Burke, M. Ernzerhof, Generalized gradient approximation made simple, Physical review 26 21
	letters, 77 (1996) 3865.
27 22 28 23	[48] C. Baerlocher, L.B. McCusker, Database of Zeolite Structures (accessed 2020-03-04). http://www.iza-structure.org/databases/
29 24	[49] B.C. Knott, C.T. Nimlos, D.J. Robichaud, M.R. Nimlos, S. Kim, R. Gounder, Consideration of the Aluminum 30 25 Distribution in Zeolites in Theoretical and Experimental Catalysis Research, ACS Catalysis, American Chemical 31 26 Society, 2018, pp. 770-784.
32 27 [ 34 28	50] S. Sklenak, J. Dědeček, C. Li, B. Wichterlová, V. Gábová, M. Sierka, J. Sauer, Aluminum Siting in Silicon-Rich 33 Zeolite Frameworks: A Combined High-Resolution27Al NMR Spectroscopy and Quantum Mechanics / Molecular 35
29	Mechanics Study of ZSM-5, Angewandte Chemie, Wiley, 2007, pp. 7424-7427.
51 52 53 54 55 56	

1
2
3
1
4
5
2
6
7
36 30 [51] C.T. Nimlos, A.J. Hoffman, Y.G. Hur, B.J. theoretical assessments of aluminum proximity in

- 36 30 [51] C.T. Nimlos, A.J. Hoffman, Y.G. Hur, B.J. Lee, J.R. Di Iorio, D.D. Hibbitts, R. Gounder, Experimental and 37 31 theoretical assessments of aluminum proximity in MFI zeolites and its alteration by organic and inorganic 38 32 structure-directing agents, Chemistry of Materials, 32 (2020) 9277-9298.
- 39 33 [52] M. Agote-Arán, R.E. Fletcher, M. Briceno, A.B. Kroner, I.V. Sazanovich, B. Slater, M.E. Rivas, A.W.J. Smith, P. 40 34 Collier, I. Lezcano-González, A.M. Beale, Implications of the Molybdenum Coordination Environment in MFI
- 41 35 Zeolites on Methane Dehydroaromatisation Performance, ChemCatChem, 2020, pp. 294-304.

42

- 43 36 [53] M. Newville, Larch: an analysis package for XAFS and related spectroscopies, Journal of Physics: Conference 44
- 37 Series, IOP Publishing, 2013, pp. 012007.
- 45 38 [54] F. Barath, Catalytic Activity of Reduced MoO3/ $\alpha$ -Al2O3 for Hexanes Reforming, Journal of Catalysis, 185 46 39 (1999) 1-11.
- 47 40 [55] T.N. Kovacs, D. Hunyadi, A.L.A. de Lucena, Thermal decomposition of ammonium molybdates, Journal of 48 Thermal Analysis and Calorimetry, 124 (2016) 1013-1021.
- 49 42 [56] D. Zhou, D. Ma, X. Liu, X. Bao, Study with density functional theory method on methane dehydro-
- 50 43 aromatization over Mo/HZSM-5 catalysts I: Optimization of active Mo species bonded to ZSM-5 zeolite, Journal 44 of Chemical Physics, 2001, pp. 9125-9129.
  - 45 [57] E.V. Fadeeva, N.A. Mamonov, L.M. Kustov, M.N. Mikhailov, The structure of active sites in a
  - 46 molybdenum/zeolite catalyst for methane dehydroaromatization: A DFT study, Russian Chemical Bulletin, 2013, 47 pp. 1967-1973.

Page 40 of 41

[58] D. Olson, G. Kokotailo, S. Lawton, W. Meier, Crystal structure and structure-related properties of ZSM-5, The Journal of Physical Chemistry, 85 (1981) 2238-2243.

58

## **Chemistry of Materials**

